Charmed baryon spectroscopy and light flavour symmetry from lattice QCD

Paula Pérez-Rubio,[*] Sara Collins, and Gunnar S. Bali[†]

Institute for Theoretical Physics, University of Regensburg, 93040 Regensburg, Germany

(Dated: August 14, 2015)

We determine the ground state and first excited state masses of singly and doubly charmed spin 1/2 and 3/2 baryons with positive and negative parity. Configurations with $N_f = 2 + 1$ non-perturbatively improved Wilson-clover fermions were employed, with the same quark action also being used for the valence quarks, including the charm. The spectrum is calculated for pion masses in the range $M_\pi \sim 259 - 460$ MeV at a lattice spacing $a \sim 0.075$ fm. Finite volume effects are studied comparing lattices with two different linear spatial extents (1.8 fm and 2.4 fm). The physical point is approached from the SU(3) limit keeping the flavour averaged light quark mass fixed. The baryon masses are extrapolated using expansions in the strange-light quark mass difference. Most particles fall into the expected SU(3) multiplets with well constrained extrapolations, the exceptions having a possibly more complex internal structure. Overall agreement is found with experiment for the masses and splittings of the singly charmed baryons. As part of the calculation an analysis of the lower lying charmonium, D and D_s spectra was performed in order to assess discretisation errors. The gross spectra are reproduced, including the D_{s0}^*, D_{s1} and D_1 mesons, while at this single lattice spacing hyperfine splittings come out $10 - 20$ MeV too low.

PACS numbers: 12.38.-t,12.38.Gc,14.20.Lq,14.40.Lb

---

[*] paula.perez-rubio@ur.de
[†] Adjunct Faculty: Tata Institute of Fundamental Research, Homi Bhabha Road, Mumbai 400005, India

I. INTRODUCTION

Heavy baryons combine relativistic light quarks and non-relativistic heavy quarks and may have similarities with heavy light mesons and, in the case of doubly charmed baryons, also quarkonia. These particles can be understood using a number of theoretical tools, in particular, Heavy Quark Effective Theory (HQET) [1, 2], non-relativistic QCD (NRQCD) [3, 4] and potential NRQCD (pNRQCD) [5, 6]. Currently, 19 charmed baryons and 8 bottomed baryons are present in the PDG summary tables[1][7]. Shortly after the discovery of the J/ψ, the first charmed baryon was detected in 1975, the Λ_c^+, at the BNL [8], followed by the discovery of Σ_c^{++} in 1976 at FNAL [9] and the first bottomed baryon, the Λ_b in 1981 at CERN [10]. In the last decade, bottomed baryons were studied at the Tevatron and more recently at the LHC, whereas charmed baryons were mainly discovered at the B-factories. While masses, lifetimes, widths and form factors have been measured, direct spin and parity identification is often still missing (they are assigned from quark model considerations). This situation will probably improve with the study of angular distributions of particle decays in LHC data thanks to the large statistics. In the future, the Belle-II experiment at SuperKEKB and the PANDA experiment at the FAIR facility will study singly charmed baryons. With respect to doubly charmed baryons, the prospects are not so promising. Only SELEX published evidence for the $\Xi_{cc}^+(3520)$ [11, 12] and its isospin partner $\Xi_{cc}^{++}(3460)$ [13], with no further confirmation by any other experiment. Besides the experimental findings, various theoretical approaches have been employed. Among these are studies based on quark models [14–22], HQET [23], QCD sum rules [24–29] and lattice QCD, using the quenched approximation [30–34] and, more recently, including sea quarks [35–44].

While most previous studies have focused on post- and prediction of the charmed baryon spectrum, in this work we investigate the light flavor dependence of the singly and doubly charmed states. Observed spectra of mesons and baryons have long been understood in terms of flavor symmetry, with, for the example of three light quark flavors ($N_f = 3$ corresponding to up, down and strange), the mesons falling into singlets and octets and the baryons into octets and decuplets. While SU(2) isospin symmetry is reasonably well respected in nature, SU(3) flavor symmetry is not. The pattern of symmetry breaking for the latter can be derived by expanding about the flavor symmetric limit in the strange-light quark mass difference ($\delta m_\ell = m_s - m_\ell$). This leads to the Gell-Mann–Okubo relations [45, 46], which are found to hold within a few per cent. Enlarging the symmetry group to SU(4) to include the charm quark provides indications of what charmed mesons and baryons should exist, however, the mass spectra may be best explained by treating charm quarks as spectators and considering the SU(3) symmetry breaking pattern as for the light hadrons.

In the past, studying the flavor structure of hadrons on the lattice was mostly restricted to approaching the physical point, keeping the strange quark mass approximately constant (and consistent with experiment) while reducing the up/down quark mass. Extrapolations to the physical point, if necessary, are guided by chiral perturbation theory, which is of uncertain validity in the range where lattice results are generated depending on the observable [47]. Recently, the QCDSF collaboration adopted an alternative strategy [48, 49] where, starting from the $N_f = 3$ theory, one approaches the physical point keeping the average quark mass fixed. This enables one to derive the quark mass dependence of physical quantities à la Gell-Mann–Okubo. The extrapolation to the physical point is limited by the order of the expansion required relative to the number and precision of the data points available to fix the corresponding coefficients. The incorporation of an additional valence quark, for example, the charm, into this framework is described in [49]. In this work, we study the flavor dependence of singly and doubly charmed baryons at a single lattice spacing for both positive and negative parity states treating the charm quark as a spectator, with the view to performing a larger scale analysis on CLS ensembles [50] including a continuum extrapolation. For the associated Gell-Mann–Okubo relations to be applicable, the charmed baryons must fall into the expected SU(3) multiplets. With only a few exceptions we find this to be the case. The SU(4) representations naturally suggest interpolators for creating (and destroying) the baryon states. We also compare these interpolators with another basis derived from HQET. Similar results for both bases are obtained for positive parity states, while differences are found for negative parity states. For the latter, some channels are obscured by the presence of two-particle scattering states of the same quantum numbers. We carefully study this as well.

The article is organized as follows. A description of our computational setup is given in Section II. This includes a discussion of the leading $\mathrm{O}(a^2)$ discretization effects, which could be significant as the simulations were performed on ensembles at a single lattice spacing $a \sim 0.075$ fm for which the charm quark mass in lattice units is around 0.4. We attempt to quantify these effects by comparing results for the lower lying charmonium and D/D_s states to experiment. In Section III we motivate our basis of interpolators for the correlation functions, followed by a discussion of the methodology used to extract the mass spectrum and the efficacy of our interpolator basis in Section IV. The charm quark is partially quenched in this study (it does not appear in the sea) and as such must be tuned to reproduce experiment on each ensemble. This procedure is described in Section V. We remark that for transparency and in order to maximize the predictive power of our simulations, we try to make use of as little experimental input as possible. For instance, we predict the absolute meson and baryon masses using one and the same value of the charm quark mass, rather than quoting splittings relative to a reference mass, such as that of the η_c meson. Comparing two volumes, we also investigate finite volume effects in Section VI A. The main result of the paper, the extrapolation to the physical point of the charmed baryon spectrum is given in Sections VI B and VI C and for the mass splittings in Section VI D, before

---

[1] With 3 star status or higher.

comparing with other recent lattice determinations in Section VI E. We finish with some concluding remarks in Section VII. Additional details are provided in Appendices A (meson effective masses), B (finite volume effects), C and D (derivation of the Gell-Mann–Okubo expressions) and E (fit ranges and extrapolations).

II. SIMULATION DETAILS

We have employed SLiNC (**S**tout **Li**nk **N**on-perturbative **C**lover) [51] $N_f = 2 + 1$ gauge configurations, generated by the QCDSF collaboration [48, 49]. The gluonic action is tree level Symanzik improved and the fermionic action has a single level of stout smearing in the hopping terms and unsmeared links in the clover term. The clover coefficient was determined non-perturbatively. The quark masses were chosen by finding the SU(3) symmetric point where the average octet pion mass, $X_\pi = \sqrt{(M_\pi^2 + 2M_K^2)/3}$, coincides with experiment. M_π and M_K correspond to the pion and kaon masses, respectively. The strange and light sea quark masses are then varied so as to approach the physical point keeping the singlet quark mass, $\overline{m} = \frac{1}{3}(2m_\ell + m_s)$ fixed up to O(a) corrections. The ensembles used in this work include several pion masses and two volumes for a single lattice spacing, see Table I. Note that the physical SU(3) symmetric value $M_\pi = M_K \approx 411$ MeV was somewhat missed. Below, we discuss our strategy for correcting for the "wrong" trajectory in the mass plane and also quantify the size of discretization errors in spectral quantities. In order to reduce auto-correlations, a single measurement was performed per configuration where the position of the source was randomly chosen and consecutive configurations are separated by two trajectories.

κ_ℓ	κ_s	κ_{c_1}	κ_{c_2}	$L/a \times T/a$	M_π (MeV)	M_K (MeV)	LM_π	$N_{\rm meas}$	a_{w_0} (fm)	a_{r_0} (fm)	$a_{\rm 1S-1P}$ (fm)
0.12090	0.12090	0.11065	0.1116	24×48	471	471	4.3	2747	0.0756(10)	0.076(2)	
0.12100	0.12070	0.11065	0.1116	24×48	394	493	3.6	1018		0.076(2)	
0.12104	0.12062	0.11065	0.1116	24×48	364	507	3.3	934		0.076(2)	
0.12090	0.12090	0.1110	0.1116	32×64	461	461	5.6	875	0.0748(9)		0.072(4)
0.12104	0.12062	0.1110	0.1116	32×64	355	499	4.3	989	0.0742(8)		0.068(4)
0.121145	0.120413	0.1110	0.1116	32×64	259	530	3.2	885	0.0746(9)		0.075(4)

TABLE I. Details of the ensembles used. κ_ℓ, κ_s and $\kappa_{c1/c2}$ correspond to the light (u/d), strange and charm quark mass parameters, respectively, and the gauge coupling is the same in all cases, $\beta = 10/g^2 = 5.5$. $N_{\rm meas}$ indicates the number of measurements used for the analysis. The last three columns indicate the values of the lattice spacing for the different ensembles, determined through w_0, r_0 and the 1S - 1P charmonium splitting. Note that the lattice spacing determinations were performed using different numbers of configurations than those used in the spectroscopy analysis.
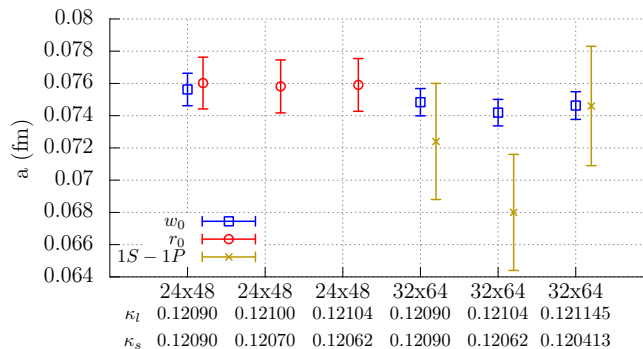

FIG. 1. The lattice spacing determined via w_0, r_0 and the 1P-1S charmonium splitting for each ensemble.

The valence charm quark is treated relativistically using the SLiNC action. We employed two different values of the mass parameter for each set of configurations, given in Table I. These were chosen so that we could interpolate to the physical charm quark mass determined by comparing the spin-averaged 1S charmonium mass to experiment (see Section V). In order to convert dimensionless lattice results to physical units the lattice spacing must be determined. We considered three quantities to set the scale: the spin-averaged 1P-1S charmonium splitting, the Sommer scale, r_0 [52] (where we used $r_0 = 0.50(1)$ fm) and the Wilson flow observable w_0 [53], which is related to t_0 [54]. Fig. 1 shows the results for each quantity, where available. The values obtained are reasonably consistent across the ensembles and also from the different observables. We take $a = 0.075$ fm without quoting an error [2], since the systematics due to the lack of a continuum limit extrapolation will induce a larger uncertainty.

———————

[2] Note that we take the continuum limit value of w_0 at physical quark masses. Therefore the precise lattice spacing is ambiguous up to a few percent.

Our value of a is about 10% smaller than the value given in Refs. [48, 49] ($a \sim 0.083$ fm) which was set from the flavor singlet baryon mass QCDSF obtained. However, it is consistent with a later determination by QCDSF [55] ($a \sim 0.073(2)$ fm). Note that the smaller lattice spacing means our values for the pion masses given in Table I differ from those of Refs. [48, 49]. In addition, the average octet pion mass, X_π, is larger than the experimental value by approximately 50 MeV ($V = 32^3 \times 64$). Recall that $\overline{m}$ is kept fixed in our simulations and $X_\pi = X_\pi(\overline{m})$ is approximately constant as $\delta m_\ell = m_s - m_\ell$ is varied from the flavor symmetric point ($\delta m_\ell = 0$) to the physical value $\delta m_\ell^{\text{phys}}$, where $(M_K^{\text{sim}})^2 - (M_\pi^{\text{sim}})^2 = (M_K^{\text{phys}})^2 - (M_\pi^{\text{phys}})^2 \approx 0.225$ GeV^2. This means that an extrapolation to the physical pion mass will result in an unphysically heavy kaon, as illustrated in Fig. 2 (point C). SU(3) mass multiplets are extrapolated via Taylor expansions in δm_ℓ starting from the flavor symmetric point such that an individual hadron mass has the dependence $M = M_0(\overline{m}) + c\delta m_\ell + O(\delta m_\ell^2)$. Note that the linear coefficient of this expansion (c) does not depend on $\overline{m}$ and, up to quadratic corrections, $M_0(\overline{m}) \approx X_{\text{multiplet}}$. The latter quantity denotes the flavor average for the given multiplet. In order to make contact with the physical theory we extrapolate masses within each SU(3) multiplet to $\delta m_\ell^{\text{phys}}$ (point B in Fig. 2) and then shift these masses by an estimate of $X_{\text{multiplet}}^{\text{phys}} - X_{\text{multiplet}}^{\text{sim}}$ (i.e. moving from B to A in Fig. 2). This procedure is described in more detail in Section VI B.
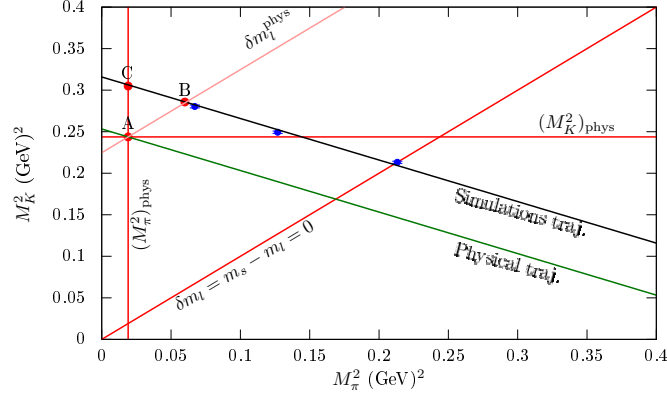

FIG. 2. The pion and kaon masses squared in physical units, using $a = 0.075$ fm, for our ensembles (blue circles) compared to the physical trajectory. The point A indicates the physical pion and kaon masses, while B indicates the point on the simulation trajectory corresponding to the physical value for $\delta m_\ell = m_s - m_\ell$ and C shows the (unphysically heavy) kaon mass corresponding to physical pion mass (but unphysical δm_ℓ).

Particles	Operators
η_c, D, D_s	$\bar{q}_1 \gamma_5 q_2$
$J/\psi, D^*, D_s^*$	$\bar{q}_1 \gamma_i q_2$
$\chi_{c0}(1P), D_0, D_{s0}$	$\bar{q}_1 q_2$
D_1, D_{s1}	$\bar{q}_1 \gamma_i \gamma_5 q_2, \bar{q}_1 \epsilon_{ijk} \gamma_j \gamma_k q_2$
$\chi_{c1}(1P)$	$\bar{q}_1 \gamma_i \gamma_5 q_2$
$h_c(1P)$	$\bar{q}_1 \epsilon_{ijk} \gamma_j \gamma_k q_2$

TABLE II. The meson interpolators employed to calculate the charmonium, D and D_s spectra.

For the SLiNC action the leading discretization effects are of O (a^2). The combination O $((m_c a)^2)$ may be significant for some quantities given that $am_c \sim 0.4$ in our simulation. In order to gauge the size of the corresponding systematic uncertainty we have computed the low-lying charmonium, D_s and D spectra for the $V = 32^3 \times 64$ ensembles using the interpolators given in Table II. Correlators constructed from these interpolators with quarks smeared over different spatial extents were combined with the variational method (see Section IV) to extract the ground state. The extrapolation to the physical point is discussed in Sections VI B and VI C, the results are presented in Fig. 3 and Table III.

Overall the radial and orbital excitations are reasonably well reproduced. This is to be expected since the typical energy scale for the 1P–1S and 2S–1S splittings in heavy-light systems is $\overline{\Lambda} \sim 0.5$ GeV, which is much smaller than the inverse lattice spacing. Similarly, for the charmonium ground state the corresponding energy scale is $m_c v_c^2 \sim 0.5$ GeV for $v_c^2 \sim 0.4$ [56]. We find for charmonium that the $\eta_c(2S)$, $\psi(2S)$, χ_{c1} and h_c states lie $50 - 60$ MeV below experiment corresponding to $2 - 3.7$ standard deviations. However, as discussed below, the 2S and 1P fine structure splittings are reproduced, albeit with large errors. It is likely that other systematics, in particular, finite volume effects are important for these radial and orbital excitations. These systematics are not investigated for mesons in this paper, however, finite volume effects for the charmed baryons are discussed in Section VI A.
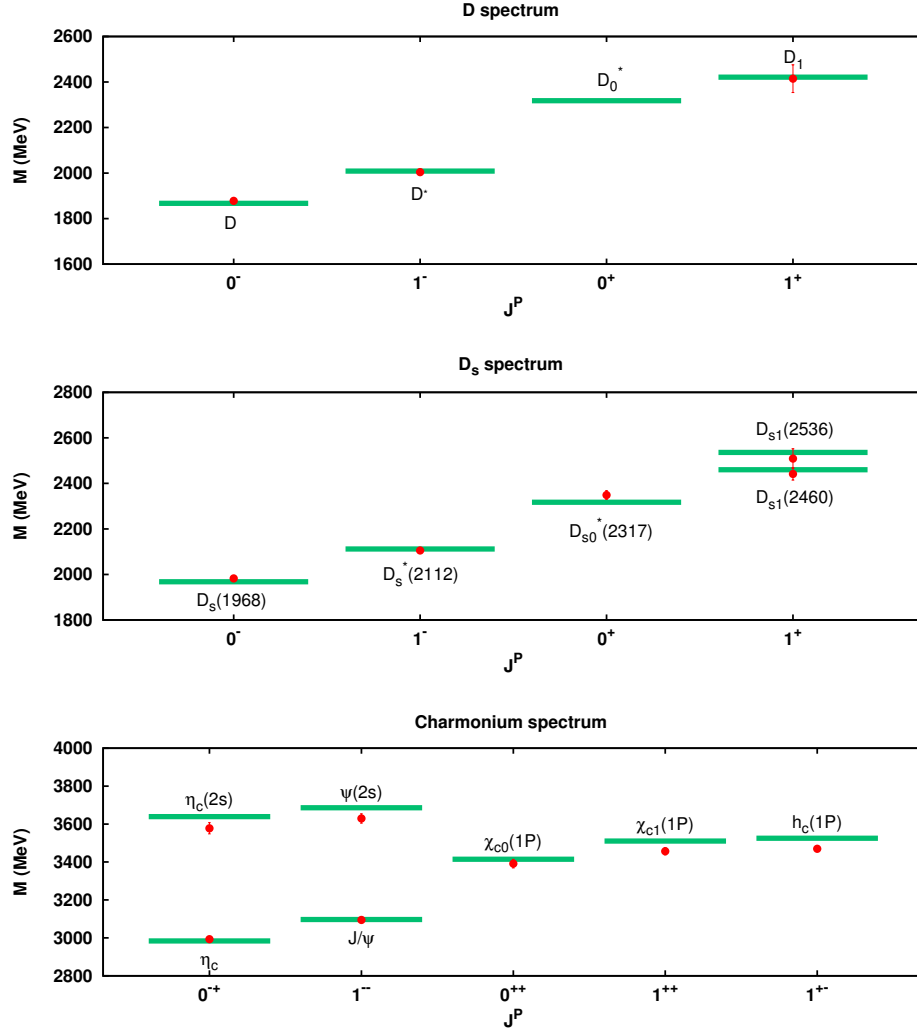
FIG. 3. The low lying D (top), D_s (middle) and charmonium (bottom) spectra at the physical point for the $V = 32^3 \times 64$ ensembles. See Sections VI B and VI C for details on how the results at the physical point are obtained.

Channel	J^{PC}	M (GeV)	Channel	J^{PC}	M (GeV)
η_c	0^{-+}	2.9929(12)	$D_s(1968)$	0^-	1.9824(85)
$\eta_c(2s)$	0^{-+}	3.5778(296)	$D_s^*(2112)$	1^-	2.1054(95)
J/ψ	1^{--}	3.0944(19)	$D_{s0}^*(2317)$	0^+	2.3490(191)
$\psi(2s)$	1^{--}	3.6294(246)	$D_{s1}(2460)$	1^+	2.4415(271)
χ_{c0}	0^{++}	3.3914(228)	$D_{s1}(2536)$	1^+	2.5092(431)
χ_{c1}	1^{++}	3.4570(192)	D	0^-	1.8778(106)
h_c	1^{+-}	3.4697(150)	D^*	1^-	2.0041(142)
			D_1	1^+	2.4147(610)

TABLE III. The low lying open and hidden charm meson spectra at the physical point for the $V = 32^3 \times 64$ ensembles.

For the 0^+ and 1^+ heavy-light mesons that are above or close to strong decay thresholds one needs to consider the relevant scattering states. We are able to resolve two closely lying states for the D_{s1} by using two interpolators (see Table II) in addition to multiple smearings in the variational method. However, a proper finite volume analysis would be required to identify the true nature of the higher lying state as the D^*K threshold lies between the $D_{s1}(2460)$ and the $D_{s1}(2546)$. For the D_1 the same analysis showed the lowest eigenvalue of the variational method to be clearly consistent with $D^*\pi$, and the next level to be compatible with experiment (the latter shown in Fig. 3), higher eigenvalues were much larger in mass. As for the D_{s1}, from heavy quark symmetry one expects two states close together [57–59] and in experiment there is the $D_1^0(2420)$ (width 27.4(2.5) MeV [7]) and the $D_1^0(2430)$ (width 384^{+130}_{-110} MeV [7]). However, a larger basis, including interpolators with derivatives, would be required to resolve the additional level. For the 0^+, only one state is expected and our results from a single scalar operator are compatible

with experiment for the D_{s0}^* within 2σ. Exchanging the strange quark for an up/down quark, the lowest eigenvalue of the D_0^* is consistent with $D\pi$. Unfortunately, we were not able to reliably extract the second eigenvalue for this channel and so we do not include a value in Fig. 3. A more extensive analysis of open and hidden charm mesons with a larger set of interpolators, including also $J = 2$ states, will be presented in a forthcoming publication. We note that studies of open charmed meson channels near thresholds including four quark interpolators have already been performed, see Refs. [60, 61].

Fine structure splittings are dominated by higher energy scales ($\mathrm{O}(m_c v_c)$ and $\mathrm{O}(m_c)$ in charmonium and the D/D_s systems, respectively) and are therefore more sensitive to discretization effects. We find $M_{J/\psi} - M_{\eta_c} = 100.1(1.5)$ MeV, $M_{D_s^*} - M_{D_s} = 122.0(2.6)$ MeV and $M_{D^*} - M_D = 126.8(10.1)$ MeV. These splittings are approximately 13 MeV, 22 MeV and 15 MeV below experiment, respectively. Assuming lattice spacing effects are the main cause for the discrepancies, we estimate $10 - 20$ MeV as the likely size of this systematic in the charmed baryon spectra (in particular for spin splittings)[3]. For most observables the total error of our final results after extrapolation to the physical point is of a comparable or larger size. For the radial and orbital excitations in charmonium, the wave function will be broader, suggesting smaller lattice spacing effects. We find the 2S hyperfine splitting, $\psi - \eta_c = 48(20)$ MeV and the 1P splitting, $\chi_{c1} - h_c = 11(19)$ MeV, compared to 46.7 MeV and 14.8 MeV, respectively, in experiment.

III.   CHARMED BARYONS AND INTERPOLATORS

The simplest way to see which charmed baryons are likely to exist is to consider the irreducible representations of the tensor product of three SU(4) fundamental representations:

$$\mathbf{4} \otimes \mathbf{4} \otimes \mathbf{4} = \mathbf{20_S} \oplus \mathbf{20_M} \oplus \mathbf{20_M} \oplus \mathbf{\overline{4}_A}. \tag{1}$$

This flavor symmetry is not respected in nature, however, the number of baryons and their flavor quantum numbers may be reproduced. Fig. 4 displays the totally symmetric 20_S-plet, the mixed symmetry 20_M-plet and the total anti-symmetric anti-quadruplet, $\overline{4}_A$. For each state within a multiplet the total spin and parity is the same and resonances may also be expected to fall into this pattern. The ground state 20_S and 20_M-plets have positive parity (consistent with the light baryon members of the multiplets) and $J = \frac{3}{2}$ and $J = \frac{1}{2}$, respectively, while the $\overline{4}_A$ ground states, in the non-relativistic limit, require non-zero orbital angular momentum and have negative parity ($J^P = \frac{1}{2}^-$). Orbital angular momentum is also needed for the negative parity counterparts to 20_S and 20_M. The lowest mass members of the SU(4) multiplets are the familiar decuplet, octet and singlet of SU(3) symmetry. The singly charmed baryons can form SU(3) sextets and anti-triplets ($\mathbf{3} \otimes \mathbf{3} = \mathbf{6_S} + \mathbf{\overline{3}_A}$), where the restriction of a totally anti-symmetric wavefunction means that there is no anti-triplet within the 20_S-plet. The doubly charmed baryons are all in SU(3) triplets.

In nature, where SU(3) flavor symmetry is broken, the physical states may not fall exactly into the expected multiplets, for example, the Ξ_c (Ξ_c') may contain a small contribution from the sextet (anti-triplet). Furthermore, the above picture does not include possible non-quark-model states. However, the observed charmed baryon spectra, with either measured J^P or assignment from potential model predictions (for a review see, for example, Ref. [62]) seem to reproduce the expected pattern: replacing a strange quark by a light quark, splittings are similar within a given SU(3) multiplet, consistent with a constituent quark model picture. We remark that since we are simulating QCD in the isospin limit ($m_u = m_d$ and omitting QED effects) then all states within an isospin multiplet are degenerate.

---

[3] We note that there is an additional uncertainty arising from the scale setting of a few percent in the splittings.
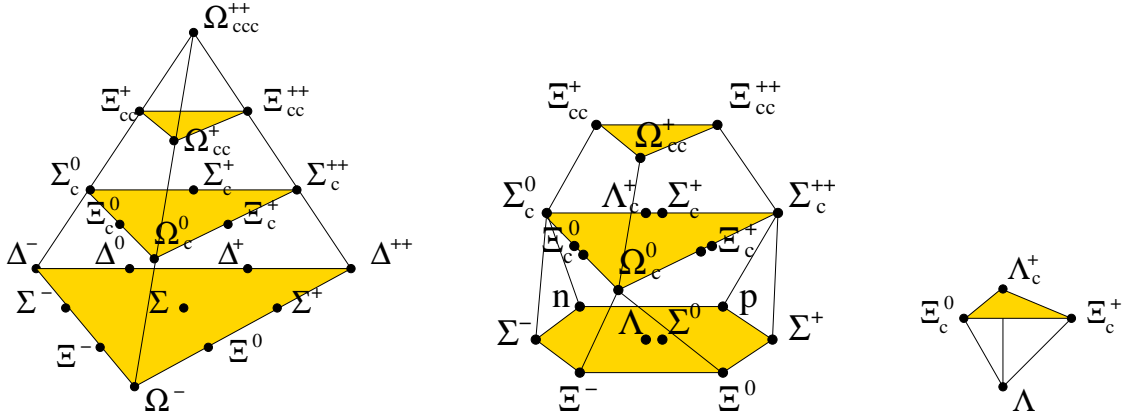
FIG. 4. The SU(4) irreducible representations for baryons: (left) the totally flavor symmetric 20_S-plet, (middle) the mixed symmetry 20_M-plet and (right) the totally anti-symmetric anti-quadruplet.

The internal structure of baryons containing light ($q \in \{\ell, s\}$) and heavy quarks (Q) can be addressed in terms of HQET and, for the QQq case, pNRQCD, starting from the static limit. At finite heavy quark masses also NRQCD is valid for doubly heavy systems. In the case of Qqq baryons, the heavy quark Q provides a color source for the two light quarks. In the $m_Q \to \infty$ limit, the light quarks have a definite total angular momentum and a total spin $s_d = 0$ or 1, corresponding to a flavor anti-symmetric or symmetric structure, respectively. In this limit, the spin splittings between baryons with $s_d = 1$ and $s_d = 0$ vanish since they are of $\mathrm{O}(\overline{\Lambda}^2/m_Q)$, where $\overline{\Lambda}$ is the energy scale of the light degrees of freedom.

For doubly heavy baryons, in what we call the HQET picture, the two heavy quarks form a diquark of small spatial extension that interacts with the light quark in analogy to heavy-light mesons (if the QQ diquark is in a color anti-triplet), shown in Fig. 5. HQET corresponds to pNRQCD in the limit of the distance between the two heavy quarks, $r \to 0$. Assuming such a QQ diquark, to leading non-trivial order in $1/m_Q$, one can show that QQq baryon spin-splittings, $M_{QQq}(J = \frac{3}{2}) - M_{QQq}(J = \frac{1}{2})$, are $3/4$ times the corresponding $\overline{Q}q$ fine structure splitting, $M_{\overline{Q}q}(J = 1) - M_{\overline{Q}q}(J = 0)$ [63].

Alternatively, the doubly heavy baryons could be comprised of a heavy and a light quark in a (color-anti-triplet) diquark and, together with the remaining heavy quark, one has a charmonium-like system, also shown in Fig. 5. In this case the level splittings can be understood in terms of pNRQCD and NRQCD, for example, the QQq spin splittings can be related to the charmonium fine structure splitting. However, this is not so straightforward as for the HQET picture since the light quark within the Qq diquark cannot be considered as spatially localized. It is possible that the HQET picture works best for the lower lying states (where $r \ll \overline{\Lambda}^{-1}$), while a charmonium-like picture is applicable for higher excitations with $r > \overline{\Lambda}^{-1}$. pNRQCD includes both possibilities.

The expected internal structure of a particle informs the choice of lattice interpolator employed, since we want to have a good overlap with the physical state. Any interpretation that is valid in the heavy quark limit may not work particularly well for charm quarks and will be more applicable to baryons involving bottom quarks. With this in mind, we implemented two sets of interpolators, those based on HQET for $J = \frac{1}{2}$ and $\frac{3}{2}$ (Table IV, where the diquark is formed from two light quarks or two heavy quarks in the case of singly and doubly charmed baryons, respectively) and also those arising from SU(4) symmetry (Table V) for $J = \frac{1}{2}$. A comparison of the efficacy of these interpolators is made in Section IV.
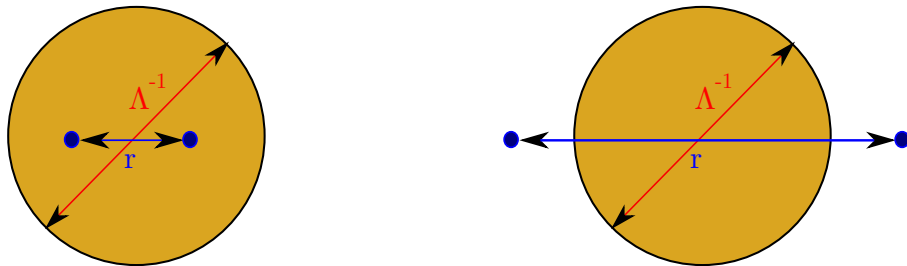

FIG. 5. Internal structure of a doubly heavy baryon: HQET picture (left hand side), Quarkonium-like (right hand side). The blue circles represent the heavy quarks, Q, and r is the average $Q - Q$ separation. In the HQET picture $r \ll \overline{\Lambda}^{-1}$, while in the charmonium picture $r \gtrsim \overline{\Lambda}^{-1}$.

The interpolators given in the tables do not have definite parity and one needs to use the projection operator $P^\pm = \frac{1}{2}(I \pm \gamma_4)$ to obtain positive or negative parity states. Since, in the non-relativistic limit, negative parity requires non-zero orbital angular momentum, interpolators including derivatives may improve the overlap with the physical states. Further exploration of the best basis will be performed in a future study. An additional projection is required for the HQET interpolators of type $\mathcal{O}_\mu$ and

HQET singly charmed baryon interpolators						
S	I	s_d	$(qq)Q$	$\mathcal{O}$	$J=\frac{1}{2}$	$J=\frac{3}{2}$
0	0	0	$(\ell\ell')c$	$\mathcal{O}_{5\gamma} = \epsilon_{abc}(\ell^{aT}C\gamma_5\ell'^b)c^c_\gamma$	Λ_c	
0	1	1	$(\ell\ell)c$	$\mathcal{O}_{\mu\gamma} = \epsilon_{abc}(\ell^{aT}C\gamma_\mu\ell^b)c^c_\gamma$	Σ_c	Σ_c^*
-1	$\frac{1}{2}$	0	$(\ell s)c$	$\mathcal{O}_{5\gamma} = \epsilon_{abc}(\ell^{aT}C\gamma_5 s^b)c^c_\gamma$	Ξ_c	
-1	$\frac{1}{2}$	1	$(\ell s)c$	$\mathcal{O}'_{\mu\gamma} = \epsilon_{abc}(\ell^{aT}C\gamma_\mu s^b)c^c_\gamma$	Ξ'_c	Ξ_c^*
-2	0	1	$(ss)c$	$\mathcal{O}_{\mu\gamma} = \epsilon_{abc}(s^{aT}C\gamma_\mu s^b)c^c_\gamma$	Ω_c	Ω_c^*
HQET doubly charmed baryon interpolators						
0	$\frac{1}{2}$	1	$(cc)\ell$	$\mathcal{O}_{\mu\gamma} = \epsilon_{abc}(c^{aT}C\gamma_\mu c^b)\ell^c_\gamma$	Ξ_{cc}	Ξ_{cc}^*
-1	0	1	$(cc)s$	$\mathcal{O}_{\mu\gamma} = \epsilon_{abc}(c^{aT}C\gamma_\mu c^b)s^c_\gamma$	Ω_{cc}	Ω_{cc}^*

TABLE IV. Quantum numbers of singly and doubly charmed baryons and interpolators, $\mathcal{O}_{A\gamma}$ in the HQET picture, where γ is the spin index. ℓ and ℓ' stand for up and down quarks, c for charm and s for strange. S, I and s_d are strangeness, isospin, and diquark total spin quantum numbers, respectively.

SU(4) singly charmed baryon interpolators				
$SU(4)$-plet	S	I	$\mathcal{O}$	$J=\frac{1}{2}$
20_M	0	0	$\mathcal{O}_{5\gamma} = \frac{1}{\sqrt{6}}\epsilon^{abc}\left\{2(\ell^{aT}C\gamma_5\ell_2'^b)c^c_\gamma + (c^{aT}C\gamma_5\ell'^b)\ell^c_\gamma - (c^{aT}C\gamma_5\ell^b)\ell'^c_\gamma\right\}$	Λ_c
	-1	$\frac{1}{2}$	$\mathcal{O}_{5\gamma} = \frac{1}{\sqrt{6}}\epsilon^{abc}\left\{2(s^{aT}C\gamma_5\ell_2^b)c^c_\gamma + (c^{aT}C\gamma_5\ell^b)s^c_\gamma - (c^{aT}C\gamma_5 s^b)\ell^c_\gamma\right\}$	Ξ_c
	0	1	$\mathcal{O}_{5\gamma} = \epsilon^{abc}(c^{aT}C\gamma_5\ell^b)\ell^c_\gamma$	Σ_c
	-1	$\frac{1}{2}$	$\mathcal{O}_{5\gamma} = \frac{1}{\sqrt{2}}\epsilon^{abc}\left\{(s^{aT}C\gamma_5 c^b)\ell^c_\gamma + (\ell^{aT}C\gamma_5 c^b)s^c_\gamma\right\}$	Ξ'_c
	-2	0	$\mathcal{O}_{5\gamma} = \epsilon^{abc}(c^{aT}C\gamma_5 s^b)s^c_\gamma$	Ω_c
SU(4) doubly charmed baryon interpolators				
20_M	0	$\frac{1}{2}$	$\mathcal{O}_{5\gamma} = \epsilon^{abc}(\ell^{aT}C\gamma_5 c^b)c^c_\gamma$	Ξ_{cc}
	-1	0	$\mathcal{O}_{5\gamma} = \epsilon^{abc}(s^{aT}C\gamma_5 c^b)c^c_\gamma$	Ω_{cc}

$\mathcal{O}'_\mu$ (see Table IV) as these contain both interpolators from $J=\frac{3}{2}$ and $\frac{1}{2}$ components. But this contribution must be disentangled using projection operators (at zero momentum):

$$(P^{3/2})_{ij} = \delta_{ij} - \frac{1}{3}\gamma_i\gamma_j, \quad i,j \in \{1,2,3\},$$

$$(P^{1/2})_{ij} = \frac{1}{3}\gamma_i\gamma_j. \tag{2}$$

We note that the interpolators for the Ξ_c and Ξ'_c states will, in principle, have an overlap with both physical states since they are not distinguished by a conserved quantum number. In the HQET case, the two interpolators differ in terms of the total spin of the diquark (s_d) which is not conserved at a finite heavy quark mass and for the SU(4) case the interpolators are in different SU(3) flavor multiplets, however, the flavor symmetry is, of course, broken. We have not taken possible mixing between the states created by the Ξ_c and Ξ'_c interpolators into account. This would require calculating the corresponding cross-correlation functions. However, such a study was performed in Ref. [43] with high statistics and no significant mixing was found. This suggests that the approximate SU(3) symmetry holds sufficiently well to suppress the mixing.

IV. VARIATIONAL METHOD AND FITTING PROCEDURE

We compute the mass spectrum in the conventional way by calculating two-point correlation functions created from sets of baryonic interpolators $\mathcal{O}_{i,\gamma}$, with spin index γ. These correlation functions contain contributions from all states with the same quantum numbers given by the interpolators

$$[C(t)]_{ij} = P^{\pm}_{\bar{\gamma}\gamma}\left\langle\mathcal{O}_{i,\gamma}(t)\overline{\mathcal{O}}_{j,\bar{\gamma}}(0)\right\rangle = \sum_n \langle 0|\mathcal{O}_{i,\gamma}(0)|n\rangle\langle n|\overline{\mathcal{O}}_{j,\bar{\gamma}}(0)|0\rangle e^{-M_n t}, \tag{3}$$

where $P^{\pm}_{\bar{\gamma}\gamma}$ is the parity projection operator. We employ the variational method [64, 65] in order to reliably extract the ground state and first excited state. For each interpolator given in Section III we generate a 3×3 matrix of correlators by varying the smearing applied to the quark fields. Extracting the eigenvalues, $\lambda^\alpha(t,t_0)$, of the generalized eigenvalue problem at large times, the lowest two states are cleanly separated:

$$C^{1/2}(t_0)C(t)C^{-1/2}(t_0)v^\alpha(t,t_0) = \lambda^\alpha(t,t_0)v^\alpha(t,t_0), \quad \lambda^\alpha(t,t_0) \propto e^{-M_\alpha(t-t_0)}\left[1 + \mathrm{O}(e^{-\Delta M_{\alpha'\alpha}t})\right], \tag{4}$$

where $\Delta M_{\alpha'\alpha} = M_{\alpha'} - M_\alpha$, and $\alpha' > \alpha$. The time-slice t_0 can be varied to reduce the excited state contamination[4] to $\lambda^\alpha(t, t_0)$ and the eigenvectors $v^\alpha(t, t_0)$. We use Wuppertal smearing [67, 68] with APE smoothed links [69, 70] where the number of Wuppertal iterations is varied to obtain one smearing combination which leads to a spatially extended interpolator with a good overlap with the ground state and two other combinations which have significant, but different, overlap with excited states. For the singly charmed baryons, the overlap of the interpolator with the physical states was most sensitive to the light quark smearing. The number of Wuppertal iterations for the heavy quark was fixed to $n = 150$ and for the light quark $n \in \{5, 25, 150\}$ was realized. For the doubly charmed baryons the situation is reversed and $n = 150$ was used for the light quark and $n \in \{5, 25, 150\}$ for the heavy quarks.
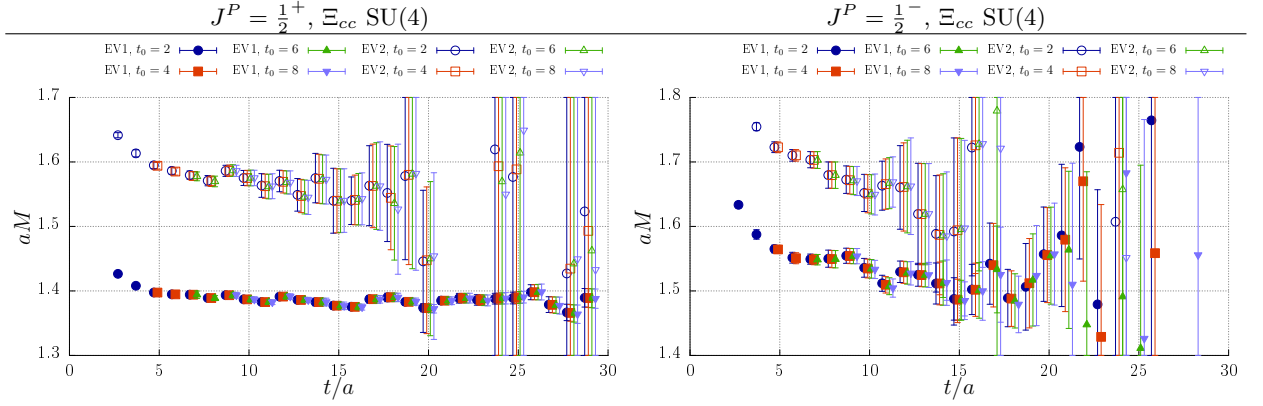

FIG. 6. Effective masses for the first (EV1) and second (EV2) eigenvalues of Ξ_{cc} for positive and negative parity obtained using different values for t_0 when solving the generalized eigenvalue problem Eq. (4) for SU(4) interpolators on the symmetric ensemble with $V = 32^3 \times 64$.

The eigenvalues $\lambda^{\alpha=1,2}(t, t_0)$ were fitted (separately) with single exponentials[5] for fixed $t_0 \geq 2a$ in the range t_i to t_f, taking the correlations between time-slices into account. The third eigenvalue was discarded as M_3 cannot be cleanly separated from higher excited states. The final fit ranges chosen, compiled in Table XI (Appendix E), have reduced correlated χ^2 values $\chi^2/\text{dof} < 2$ and in most cases $\chi^2/\text{dof} \sim 1$. For these fit ranges the masses extracted were stable within errors as t_i was further increased. No significant dependence on t_0 was found (see, for example, Fig. 6) and we take $t_0 = 2a$. The statistical errors were evaluated using the jackknife method combined with binning. Measurements were performed on every other trajectory for each ensemble and the errors were stable for $n_{\text{bin}} \geq 2 - 4$. We made the conservative choice of $n_{\text{bin}} = 4$, which is consistent with $n_{\text{bin}} > 4\tau_{\text{int}}$, where τ_{int} is the integrated auto-correlation time. The latter was estimated via the Γ-method [71, 72] to be between 0.5 and 0.7, depending on the state.

Effective masses,

$$M_\alpha(t) = \frac{1}{2a} \log\left(\frac{\lambda^\alpha(t - a, t_0)}{\lambda^\alpha(t + a, t_0)}\right), \tag{5}$$

and fits for a representative sample of states are shown in Fig. 7 for the HQET interpolators on the symmetric ensembles with $V = 32^2 \times 64$ corresponding to $M_\pi = M_K = 461$ MeV. For the positive parity states we are able to extract a reasonable signal for the first two eigenvalues for both $J = \frac{1}{2}$ and $\frac{3}{2}$. For the negative parity states, which are statistically noisier, clear ground state signals were obtained for $J = \frac{1}{2}$ and $\frac{3}{2}$, however, the first excited state was only reliably extracted for the doubly charmed baryons.

For the spin-$1/2$ particles we can compare the HQET and SU(4) interpolators. Effective masses for a state from each multiplet are shown in Fig. 8. The positive parity particles display a consistent picture: the SU(4) interpolators have a slightly better overlap with the desired states for the sextet baryons ($\Sigma_c, \Xi'_c, \Omega_c$), are only marginally better for the anti-triplet baryons (Λ_c, Ξ_c) and no difference is observed for the doubly charmed triplet (Ξ_{cc}, Ω_{cc}). The latter is due to the corresponding correlation functions only differing by terms which are suppressed in the non-relativistic limit, when expressed through upper and lower components of the quark spinors. This is not the case for singly charmed baryons nor for negative parity. Indeed, a more striking pattern emerges for negative parity. For the sextets, the SU(4) interpolators have a much better overlap with the ground state while for the triplet and (even more markedly) the anti-triplet the HQET interpolators are clearly better. For the first excitation the SU(4) interpolators provide a better signal, although there is no clear single state dominance for the singly charmed baryons.

-----

[4] For $t > t_0 \geq t/2$, only $\alpha' > N$ will contribute where N is the rank of the basis [66], a limit that we do not consider here.

[5] We assume the baryon masses to be heavy enough for the backward propagating particle to have a negligible influence.
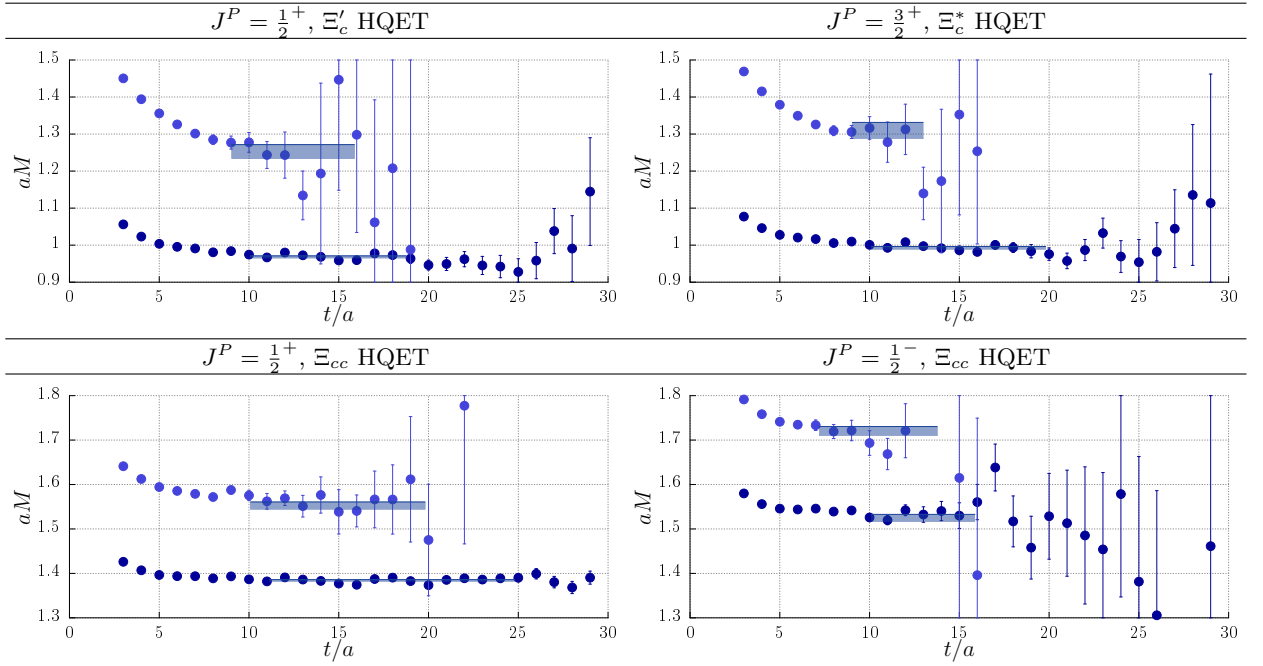
FIG. 7. Effective masses for the first and second eigenvalues for HQET interpolators on the symmetric ensemble with $V = 32^3 \times 64$. The filled regions indicate the fit ranges chosen and the fit results, including the statistical errors.

These comparisons are made with the same smearings applied to both sets of interpolators. Changing or optimizing the smearing in the individual cases may change these conclusions. The SU(4) and HQET interpolators in each channel both belong to the same (lattice) hypercubic representation: either the dimension two G_1 representation for the interpolators denoted as spin-1/2 in Tables IV and V, which in the continuum gives $J = \frac{1}{2}, \frac{7}{2}, \ldots$ or the dimension four H representation for the spin-3/2 interpolators corresponding to continuum $J = \frac{3}{2}, \frac{5}{2}, \ldots$. In the limit of very large statistics the SU(4) and HQET interpolators should give the same energy for each state. For positive parity consistency is seen, while for negative parity we use the interpolator with the best overlap for our setup. Similar behavior is seen throughout for the smaller volume, $V = 24^3 \times 48$.

Note that care has to be taken in order to avoid the misidentification of multi-particle states, for example, a positive parity baryon plus a pion as a negative parity baryon. We have studied this systematically for the ground state negative parity channels. All but one of our $J^P = \frac{3}{2}^-$ ground states are smaller in mass than two-particle states of the same quantum numbers, consisting either of a $\frac{3}{2}^+$ baryon or a $\frac{1}{2}^+$ baryon plus a pseudoscalar meson in a S-wave or a P-wave, respectively. None of the $\frac{1}{2}^-$ states contain D or D_s mesons – all combinations of these mesons with $\frac{1}{2}^+$ baryons of the same combined isospin, strange and charmness are heavier in mass. There are, however, quite a few S-wave decay channels with thresholds close to our mass estimates that require careful study, in particular

$$
\begin{array}{llll}
\Lambda_c \to \Sigma_c + \pi\,, & \Sigma_c \to \Lambda + \pi\,, & \Sigma_c \to \Sigma_c + \pi\,, & \Xi_c^* \to \Xi_c^* + \pi\,, \\
\Xi_c \to \Lambda_c + K\,, & \Xi_c \to \Sigma_c + K\,, & \Xi_c \to \Xi_c + \pi\,, & \Xi_c \to \Xi_c' + \pi\,, \\
\Xi_c' \to \Lambda_c + K\,, & \Xi_c' \to \Sigma_c + K\,, & \Xi_c' \to \Xi_c + \pi\,, & \Xi_c' \to \Xi_c' + \pi\,, \\
\Omega_c \to \Xi_c + K\,, & \Omega_c \to \Xi_c' + K\,, & \Xi_{cc} \to \Xi_{cc} + \pi\,, & \Omega_{cc} \to \Xi_{cc} + K\,,
\end{array}
$$

where the baryons on the left hand sides are implied to have negative parity and those on the right hand sides positive parity. Neither have we made the isospin nor charges explicit. Comparing all these channels at our three different sea quark mass combinations leads to the following conclusions. The ground state negative parity Ω_c state, obtained both from the SU(4) and HQET inspired interpolators, is always degenerate with the sum of the Ξ_c and a kaon. We show the corresponding effective masses at $M_\pi = X_\pi = 461$ MeV and at $M_\pi = 259$ MeV in Fig. 9. Likewise, we identify our negative parity Ξ_c' signal as a Λ_c plus kaon scattering state.

Particularly interesting is the behavior of the negative parity Λ_c, also depicted in Fig. 9 for two ensembles: while effective masses obtained from the SU(4) interpolator are degenerate with the combined mass of a Σ_c and a pion, the effective masses from the HQET interpolator are systematically lower, at least at our two heavier pion mass points. This suggests the HQET interpolator to significantly overlap with a physical state lower in mass than the scattering state while the SU(4) interpolator in this case strongly couples to the close-by two-particle state. All the other negative parity singly and doubly charmed baryons
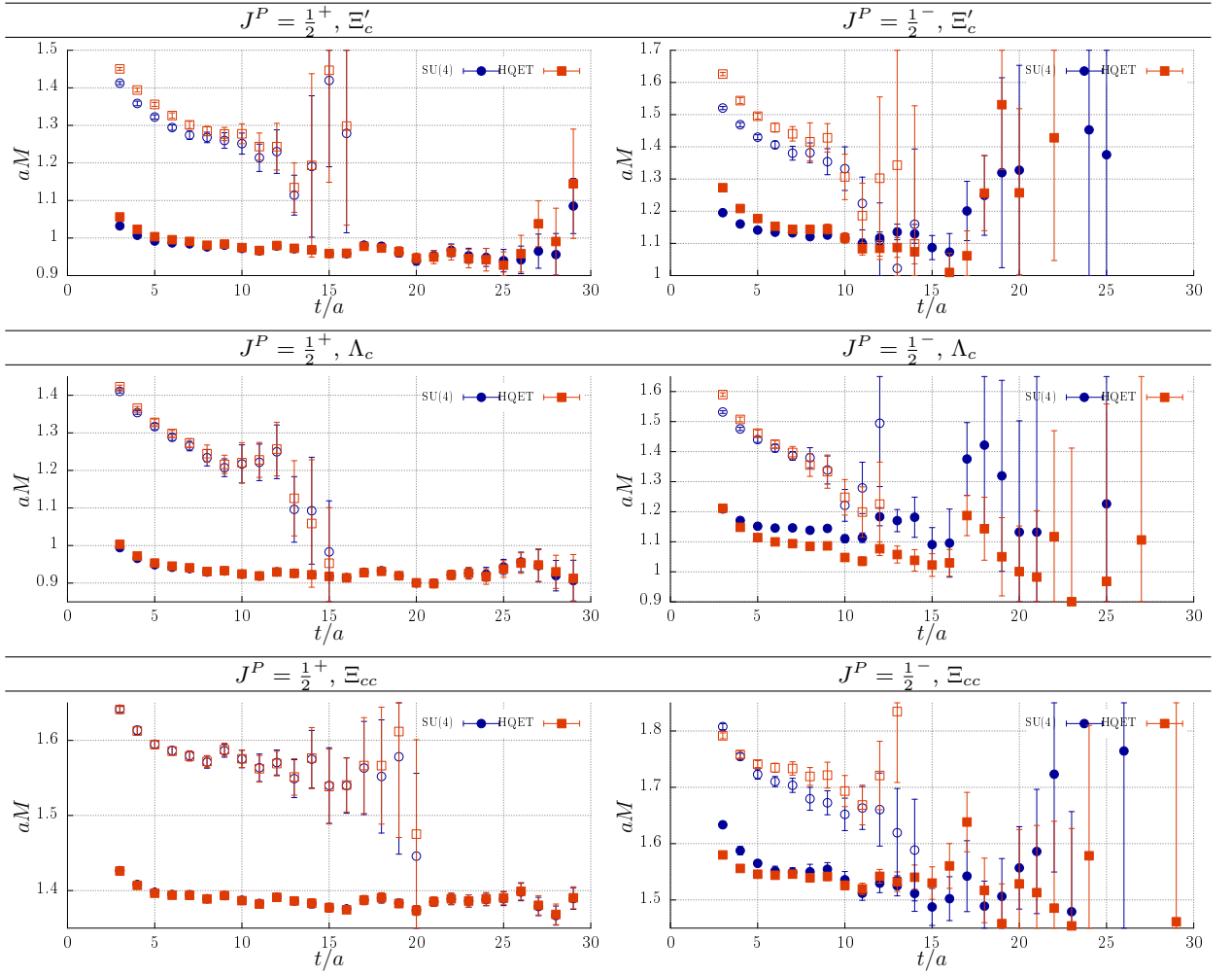
FIG. 8. Comparison of the effective masses for SU(4) and HQET interpolators employed on the ensemble at the symmetric point with $V = 32^3 \times 64$. The ground (first excited) state is indicated by filled (open) symbols.

seem to be relatively stable under strong decays or, in the few cases where their masses are higher than those of the potential decay products, at least the interpolators we employ are insensitive to the presence of these scattering states. A similar analysis for the first excitation (for both parities) is challenging due to the number of relevant two- and even three-particle states.

The lower lying meson spectrum in the charmonium, D and D_s sectors was also determined in order to estimate the size of discretization errors (as discussed in Section II) and to enable the tuning of the charm quark mass parameter (see the next Section). Except for the 1^+ D/D_s channel, we employed 3×3 correlation matrices and applied the variational method, as described above, extracting the ground state mass and in some cases the excited state for each meson. Spatially extended interpolators where constructed using $n \in \{5, 25, 150\}$ iterations of Wuppertal smearing for the charm quark, the light quarks were not smeared[6]. Effective masses and fit results for a sub-set of states are displayed in Fig. 19 in Appendix A for the symmetric larger volume ensemble. Fitting ranges for all channels are given in Table XII of Appendix E. For the 1^+ channel, two interpolators were implemented (see Table II) and a 6×6 correlation matrix was computed. This enabled us to resolve pairs of closely lying states, as illustrated in Fig. 20 (Appendix A). In terms of multi-particle states, the 0^+ and 1^+ D/D_s mesons are above/close to the $D\pi/DK$ and $D^*\pi/D^*K$ experimental thresholds, respectively. We discuss our results for these channels, also shown in Fig. 3, in Section VI B.

---

[6] Note that for meson interpolators without derivatives the smearing can be "transformed" from one quark to the other.
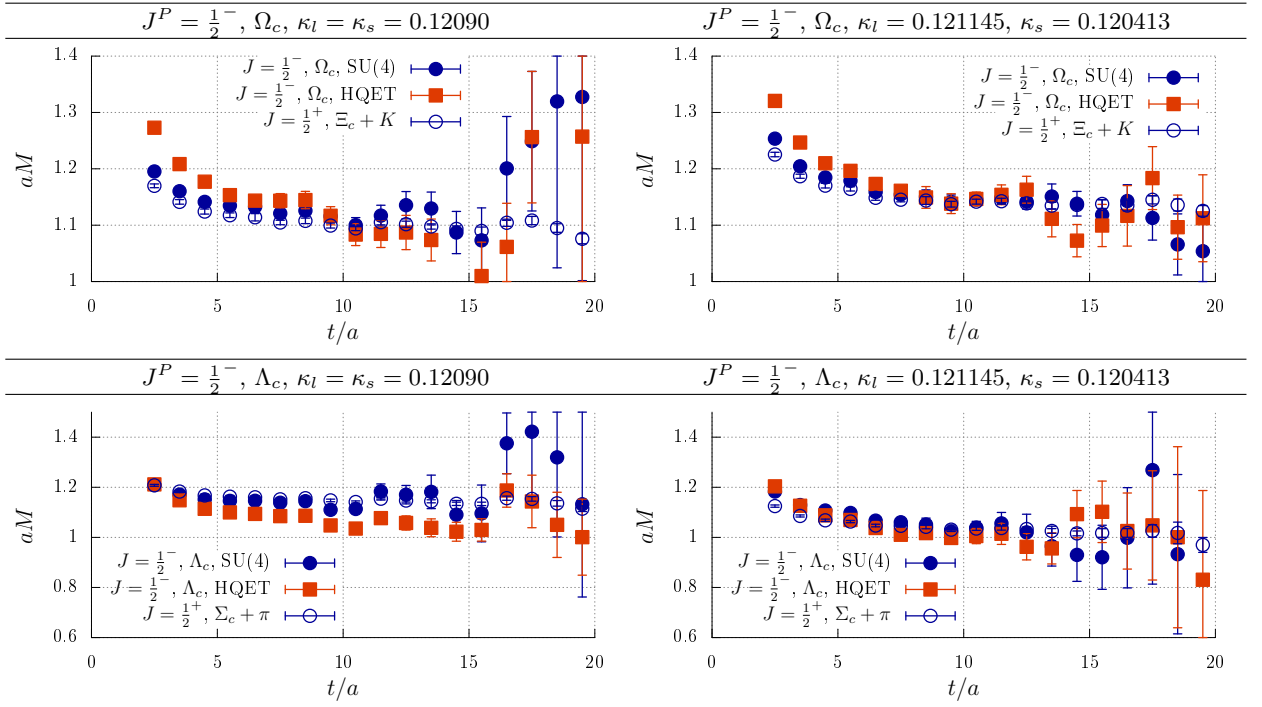
FIG. 9. Comparison of negative parity effective masses with the relevant strong decay thresholds for (top) Ω_c and (bottom) Λ_c on (left) the symmetric ensemble and (right) the most asymmetric ensemble for $V = 32^3 \times 64$.

κ_l	κ_s	$L/a \times T/a$	κ_{charm}
0.12090	0.12090	32×64	0.1114801(67)
0.12104	0.12062	32×64	0.1114869(43)
0.121145	0.120413	32×64	0.1114908(48)

TABLE VI. Final values for κ_{charm} for each ensemble determined using the $1S$ charmonium mass with full statistics.

V. TUNING OF κ_{charm}

The charm quark mass parameter, κ_{charm}, was tuned by requiring that the 1S spin-averaged charmonium mass, $M_{1\mathrm{S}} = \frac{1}{4}M_{\eta_c} + \frac{3}{4}M_{J/\psi}$ is equal to the experimental value. For this quantity the dependence on the light sea quarks is sub-leading and furthermore the associated discretization errors are likely to be reduced since contributions from fine structure interactions are removed. The tuning was performed in two stages on each $32^3 \times 64$ ensemble. Firstly, a coarse tuning involving 200 configurations separated by 2 trajectories determined a preliminary value for κ_{charm}. Two values of the mass parameter, κ_{c1} and κ_{c2} (see Table I), were chosen to bracket κ_{charm}, spaced closely enough that a linear interpolation in $1/\kappa$ to the physical point would be sufficient. In the second stage the meson and baryon spectrum was determined with full statistics for $\kappa_{c1/c2}$ and the final value of κ_{charm} determined from $M_{1\mathrm{S}}$. This mass is displayed in Fig. 10 for $\kappa_{c1/c2}$ and the results for κ_{charm} are listed in Table VI. The meson and baryon masses were then interpolated to the physical charm quark mass. Fig. 10 shows there is little dependence of $M_{1\mathrm{S}}$ at fixed $\kappa_{c1/c2}$ on the sea quark masses. This translates into very similar values for κ_{charm} across the different ensembles. The same values were employed for the smaller, $24^3 \times 48$, ensemble where the light/strange quark masses are matched. For the intermediate small volume, an interpolation was performed.

VI. RESULTS

A. Finite size effects

With two volumes available with spatial extents, $L = 24a$ and $L = 32a$, corresponding to $1.8\,\mathrm{fm}$ and $2.4\,\mathrm{fm}$, respectively, a study of finite volume effects of the charmed baryon spectrum can be attempted. The same quark mass parameters have been used for two sets of ensembles, at the symmetric point ($\kappa_{\mathrm{sym}} = 0.12090$) and the asymmetric ensemble with the light-strange combination ($\kappa_{\mathrm{asym}} = 0.12104, 0.12062$), see Table I. Differences between the masses extracted from the two volumes,
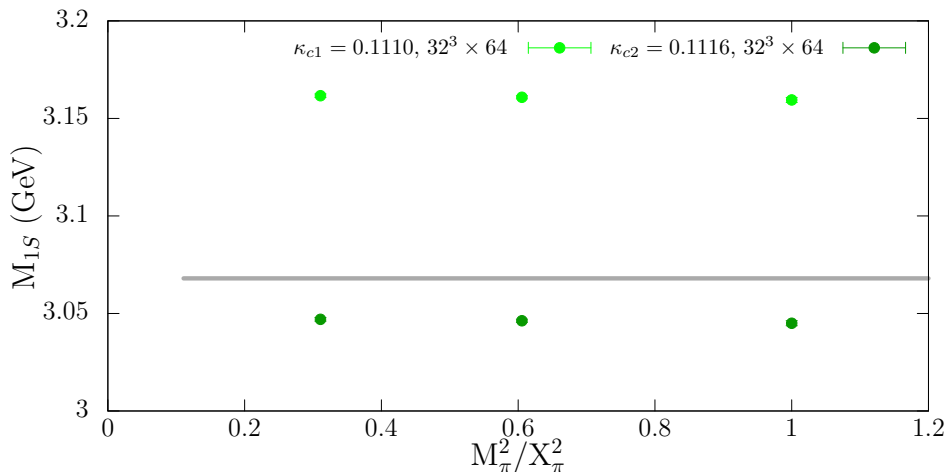
FIG. 10. The charmonium M_{1S} mass determined with $\kappa_{c1/c2}$. The horizontal line indicates the experimental value.

$\Delta M = M_{24} - M_{32}$, can be computed directly; the results are given in Tables VIII and IX in Appendix B. The mass splittings are only significantly non-zero (where we take 2.5σ to indicate significance) at the symmetric point since we have much higher statistics in this case for the smaller volume. However, similar or larger magnitudes for the difference on the asymmetric ensemble (although possibly less significant) indicate a trend. In addition, we look for consistency between the two types of interpolators, HQET and SU(4), where available and that any difference decreases if a light quark is replaced by a strange quark within a multiplet (for the asymmetric ensemble).

In general, one expects larger finite volume effects for singly charmed baryons compared to doubly charmed ones, similarly, for excited states compared to ground states. Whether the effects can be observed depends on the size of the statistical errors. Our results fit into the expected pattern. For the positive parity multiplets, we find masses are reduced by about 10–40 MeV when changing the spatial extent from 1.8 fm to 2.4 fm for the ground state sextets and the anti-triplet, while the ground state doubly charmed triplets are unchanged. The statistical errors for the excited states of the singly charmed multiplets are large and no significant finite size effects are visible apart from a small increase for the anti-triplet. However, in the doubly charmed case, with much smaller errors, clear differences of around 40–87 MeV emerge, again decreasing the mass with increasing volume. The negative parity states are less affected with only the ground state anti-triplet showing a notable decrease between $L = 24a$ and $32a$. The $J = \frac{1}{2}$ sextet and $J = \frac{3}{2}$ triplet have small positive shifts. Note that the $J = \frac{3}{2}$ negative parity sextet is not included in Table IX as we were not able to extract a reliable signal in these channels for the smaller volume. The finite volume effects for a subset of states are shown in Fig. 11.

An estimate of the size of the remaining systematic in the $L = 32a$ results can be made by assuming the finite volume dependence of the masses is of the form $M_L = M_\infty + cF(L)$, where M_∞ is the infinite volume mass and $F(L) = e^{-M_\pi L}$ is the leading order effect in the asymptotic regime and $F(L) = 1/L^3$ otherwise. This leads to

$$\Delta M_\infty = M_{32} - M_\infty = (M_{24} - M_{32})(F(24a)/F(32a) - 1)^{-1} = \Delta M \Delta F, \qquad (6)$$

where $\Delta F = 0.4$ and 0.6 for the symmetric ($\kappa_{\rm sym}$) and asymmetric ensemble ($\kappa_{\rm asym}$) in the asymptotic case, respectively, and $\Delta F = 0.7$ in the $1/L^3$ regime. Considering the values of ΔM in Table VIII, this leads to the infinite volume masses at $M_\pi = 355$ MeV being, for example, approximately 9–22 MeV smaller for the Σ_c, 11–14 MeV smaller for the Λ_c and 34–48 MeV smaller for the excited state Ξ_{cc} and Ξ_{cc}^*. At this pion mass with $L = 32a$, $LM_\pi = 4.3$, one would expect the lower bounds to apply. These estimates should be compared to the final values for the masses given in Table VII, discussed in Section VI C.

Since the lightest pion mass for the $L = 24a$ ensembles is quite large, $M_\pi = 364$ MeV, we do not attempt to extrapolate these results to the physical point and they are not included in any further analysis.

B. Extrapolation to the physical masses

An important advantage of approaching the physical point using the QCDSF strategy, starting from the flavor symmetric point and keeping the average light quark mass fixed, is that the light quark mass dependence of physical quantities is well constrained as long as flavor symmetry violations are reasonably small. The dependence of meson and baryon masses on the symmetry breaking parameter, $\delta m_\ell = m_s - m_\ell$, was derived in Ref. [49] and extending this method to include partially quenched quarks
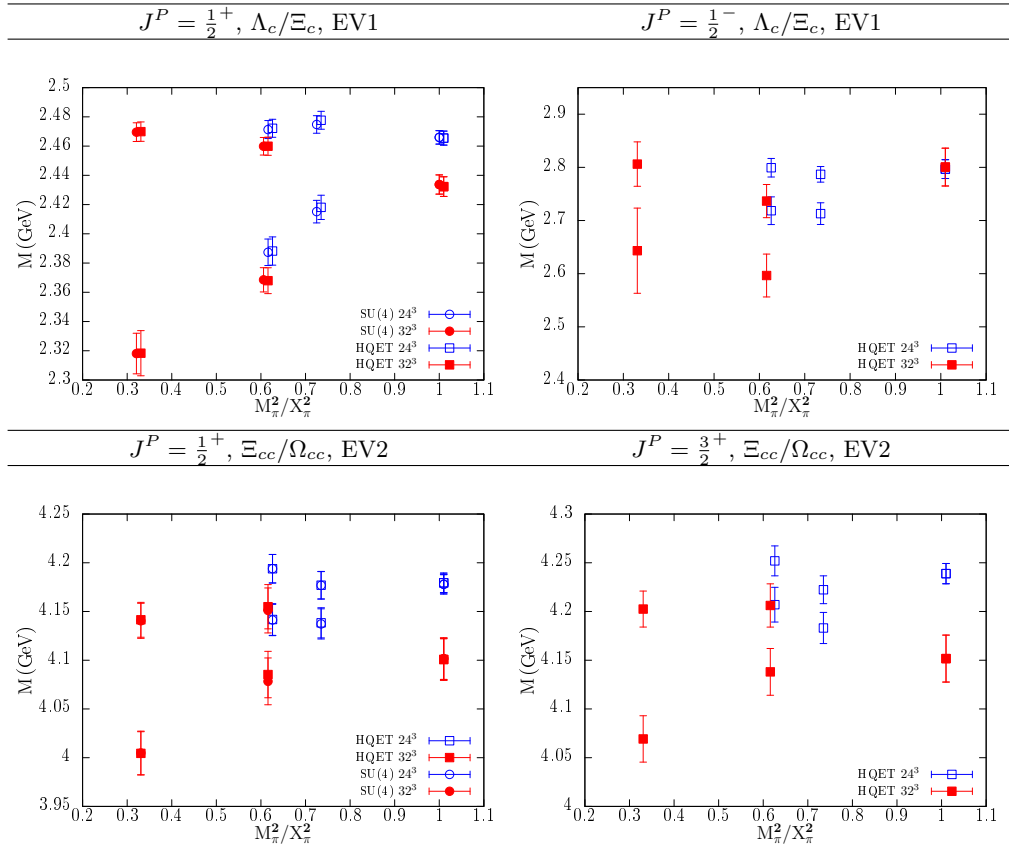
FIG. 11. Comparison of the $V = 24^3 \times 48$ and $32^3 \times 64$ results as a function of M_π^2/X_π^2 for a selection of multiplets exhibiting finite volume effects, where $1 - M_\pi^2/X_\pi^2 \propto \delta m_\ell + \mathrm{O}(\delta m_\ell^2)$. Top left and top right, the first eigenvalue (EV1) of the positive and negative parity singly charmed anti-triplet, respectively. Bottom left and bottom right, the second eigenvalue (EV2) of the positive parity doubly charmed triplet for $J = \frac{1}{2}$ and $\frac{3}{2}$, respectively.

was discussed in Refs. [49, 55]. Here, we follow an analogous approach treating the charm quark as a spectator. We classify the charmed baryons according to the SU(3) flavor symmetry multiplets for the one or two light quarks present. In the isospin limit, we have the following channels

- sextet: $(\Sigma_c, \Xi_c', \Omega_c)$ for $J = \frac{1}{2}$ and $(\Sigma_c^*, \Xi_c^*, \Omega_c^*)$ for $J = \frac{3}{2}$,

- triplet: (Ξ_{cc}, Ω_{cc}) for $J = \frac{1}{2}$ and $(\Xi_{cc}^*, \Omega_{cc}^*)$ for $J = \frac{3}{2}$,

- anti-triplet: (Λ_c, Ξ_c) for $J = \frac{1}{2}$.

The light quark mass dependence of each multiplet can be derived by considering the matrix element $\langle B_R|M|B_R\rangle$. The mass matrix $M = \overline{m}\mathbf{1} - \sqrt{3}\delta m_\ell T_8 = \overline{m}H_0 + \delta m_\ell H_8$ where T_8 is the SU(3) generator and B_R is the baryon multiplet in representation R. H_8 transforms like the eighth component of the octet representation and since $\overline{m}$ is kept constant, this is the only part of the mass matrix which is changing as we approach the physical limit. Performing a perturbative expansion in δm_ℓ we have

$$\langle B_R|M|B_R\rangle = M_0^R + \delta m_\ell \langle B_R|H_8|B_R\rangle + \delta m_\ell^2 \sum_{R' \neq R} \frac{|\langle B_R|H_8|B_{R'}\rangle|^2}{M_0^R - M_0^{R'}} + \cdots, \tag{7}$$

where $M_0^R = \overline{m}\langle B_R|H_0|B_R\rangle$ is the mass of the multiplet R in the flavor symmetric limit. In the light baryon sector the expansion to first order leads to the Gell-Mann–Okubo (GMO) relation [45, 46]. The expressions for the linear terms for the charmed baryon multiplets are derived in Appendix D. Here, we comment that the matrix elements are the flavor singlet terms arising from the decomposition of the direct products of $\overline{\mathbf{R}} \otimes \mathbf{T_H} \otimes \mathbf{R}$, where $\mathbf{T_H}$ is the representation of H. This means that the number of terms appearing at each order is given by the number of times the trivial representation appears in the direct product. At the lowest order ($\overline{\mathbf{R}} \otimes \mathbf{1} \otimes \mathbf{R}$) only one term arises, and for the sextet, triplet and anti-triplet that we are considering there is also only one term at first order ($\overline{\mathbf{R}} \otimes \mathbf{8} \otimes \mathbf{R}$). Hence, within each multiplet there is only one coefficient at $\mathrm{O}(\delta m_\ell)$ and

one can extrapolate all states within a multiplet (to this order) using just two parameters. However, at second order the trivial representation appears three (two) times for the sextet (triplet/anti-triplet) such that there are the same number of new coefficients as particles within a multiplet.

Below we display the expressions for the light quark mass dependence of the charmed baryons masses derived in Appendix D (Eqs. (D8), (D13) and (D15)). We use the GMO relations for the light mesons [48, 49]

$$M_\pi^2 = (M_0^{\mathbf{8}})^2 - \frac{2}{3}D\delta m_\ell + \mathrm{O}(\delta m_\ell^2), \tag{8}$$

$$M_K^2 = (M_0^{\mathbf{8}})^2 + \frac{1}{3}D\delta m_\ell + \mathrm{O}(\delta m_\ell^2), \tag{9}$$

and $X_\pi^2 = \frac{1}{3}(M_\pi^2 + 2M_K^2) = (M_0^{\mathbf{8}})^2 + \mathrm{O}(\delta m_\ell^2)$ to replace δm_ℓ with $(X_\pi^2 - M_\pi^2)/X_\pi^2$ ignoring $\mathrm{O}(\delta m_\ell^2)$ terms. Such higher order terms can be absorbed into the coefficients of the quadratic terms below.

Sextet, $R = \mathbf{6}$:

$$M_{\Sigma_c} = M_0^{\mathbf{6}} - \frac{2}{3}A_1 \frac{X_\pi^2 - M_\pi^2}{X_\pi^2} + A_2 \left(\frac{X_\pi^2 - M_\pi^2}{X_\pi^2}\right)^2, \tag{10}$$

$$M_{\Xi_c'} = M_0^{\mathbf{6}} + \frac{1}{3}A_1 \frac{X_\pi^2 - M_\pi^2}{X_\pi^2} + A_3 \left(\frac{X_\pi^2 - M_\pi^2}{X_\pi^2}\right)^2, \tag{11}$$

$$M_{\Omega_c} = M_0^{\mathbf{6}} + \frac{4}{3}A_1 \frac{X_\pi^2 - M_\pi^2}{X_\pi^2} + A_4 \left(\frac{X_\pi^2 - M_\pi^2}{X_\pi^2}\right)^2. \tag{12}$$

Triplet, $R = \mathbf{3}$:

$$M_{\Xi_{cc}} = M_0^{\mathbf{3}} - \frac{1}{3}B_1 \frac{X_\pi^2 - M_\pi^2}{X_\pi^2} + B_2 \left(\frac{X_\pi^2 - M_\pi^2}{X_\pi^2}\right)^2, \tag{13}$$

$$M_{\Omega_{cc}} = M_0^{\mathbf{3}} + \frac{2}{3}B_1 \frac{X_\pi^2 - M_\pi^2}{X_\pi^2} + B_3 \left(\frac{X_\pi^2 - M_\pi^2}{X_\pi^2}\right)^2. \tag{14}$$

Anti-Triplet, $R = \bar{\mathbf{3}}$:

$$M_{\Lambda_c} = M_0^{\bar{\mathbf{3}}} - \frac{2}{3}C_1 \frac{X_\pi^2 - M_\pi^2}{X_\pi^2} + C_2 \left(\frac{X_\pi^2 - M_\pi^2}{X_\pi^2}\right)^2, \tag{15}$$

$$M_{\Xi_c} = M_0^{\bar{\mathbf{3}}} + \frac{1}{3}C_1 \frac{X_\pi^2 - M_\pi^2}{X_\pi^2} + C_3 \left(\frac{X_\pi^2 - M_\pi^2}{X_\pi^2}\right)^2. \tag{16}$$

Note that for the sextet and triplet there are equivalent expressions for the $J = \frac{3}{2}$ states with different coefficients. In Refs. [49, 55] analogous parameterizations are given (but to higher order in their framework)[7]. The above forms can be applied to extrapolate our results to the physical point if the charmed baryons are regular three quark states where the charm is a spectator and the particles fall into the SU(3) flavor multiplets. As for any expansion the coefficients of the flavor symmetry breaking terms should be small and the extrapolation will be well constrained whenever only the first few terms are significant.

In this study we have the additional complication of needing to correct for the fact that the simulation trajectory misses the physical point in the $m_s - m_\ell$ mass plane (see Fig. 2). The value of $\overline{m} = \overline{m}^{\mathrm{phys}} + \Delta\overline{m}$ is off by a small amount $\Delta\overline{m}$ and this means, in the expressions above, the masses M_0 also differ from the physical ones by $M_0 = M_0^{\mathrm{phys}} + \Delta M_0$. The linear δm_ℓ expansion coefficients should be unaffected. Hence, to make contact with the physical point we extrapolate to the physical δm_ℓ defined as $M_\pi^2 = (M_K^{\mathrm{sim}})^2 - (M_K^{\mathrm{phys}})^2 + (M_\pi^{\mathrm{phys}})^2$ and then shift the masses within each multiplet by $\Delta X_{\mathrm{multiplet}} = X_{\mathrm{multiplet}}^{\mathrm{phys}} - X_{\mathrm{multiplet}}^{\mathrm{sim}} \sim \Delta M_0^{\mathrm{multiplet}}$, where $X_{\mathrm{multiplet}} \sim M_0^{\mathrm{multiplet}}$ is the flavor average for each multiplet. This procedure should be correct up to $\mathrm{O}(\Delta\overline{m}\delta m_\ell^2)$ corrections, see Eq. (7). For the singly charmed baryons we could choose

———

[7] Note that their expansion is given in terms of $m_q - \overline{m}$, which, unlike $\delta m_\ell = m_s - m_\ell$, changes when shifting $\overline{m}$.
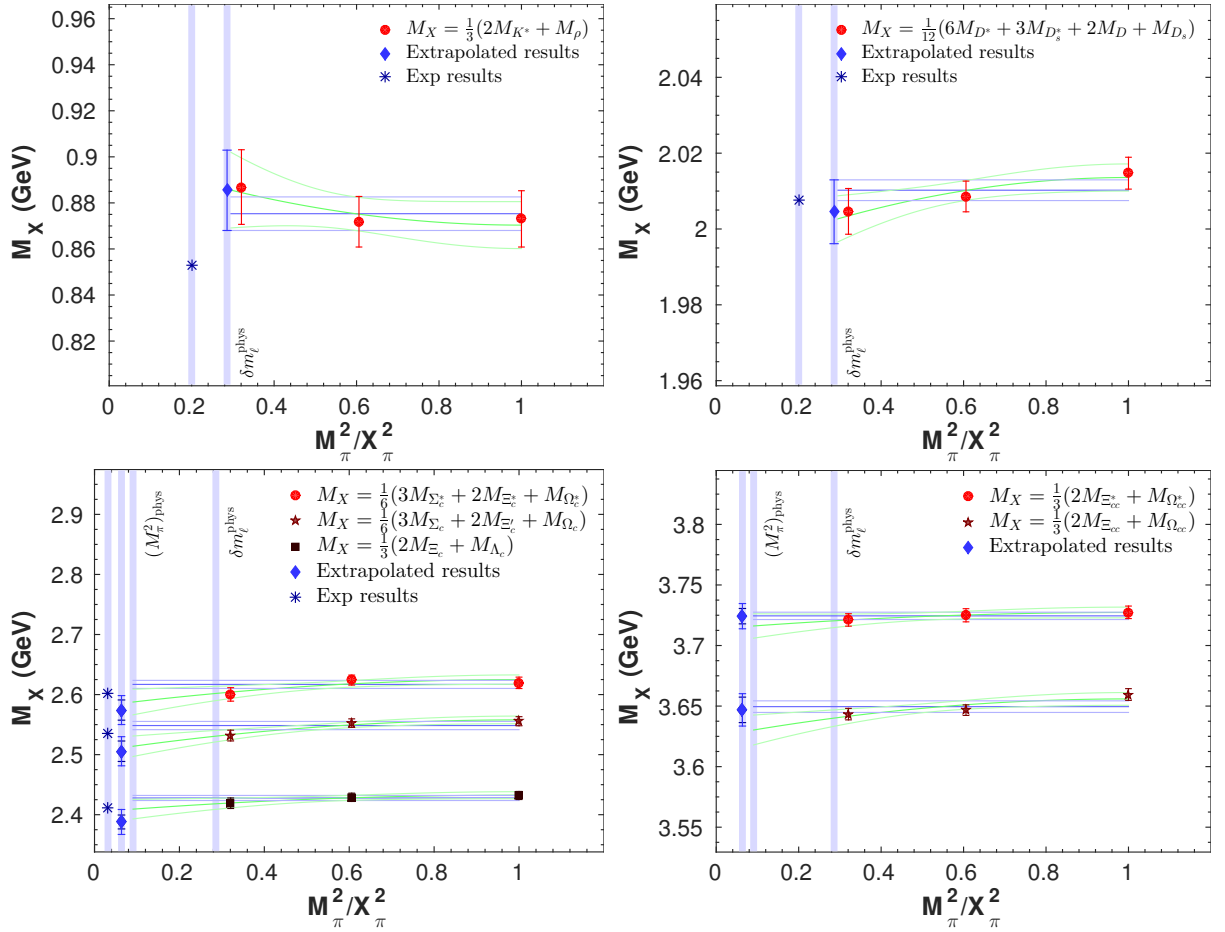
FIG. 12. Flavor invariant quantities as a function of M_π^2/X_π^2 on the $32^3 \times 64$ ensembles. Note that $1 - M_\pi^2/X_\pi^2 \propto \delta m_\ell + \mathrm{O}(\delta m_\ell^2)$. (Top left) the light vector meson and (top right) the spin averaged 1S heavy-light meson. Fits to a constant and a constant plus quadratic term in δm_ℓ are indicated along with the extrapolated values (blue diamonds) obtained at the point corresponding to physical $\delta m_\ell = \delta m_\ell^{\mathrm{phys}}$. The error on the extrapolated results incorporates both fits using Eqs. (17) and (18). The experimental results are also shown. Similarly for (bottom left) singly charmed baryons and (bottom right) doubly charmed baryons for HQET inspired interpolators. For the charmed baryons, the final values are obtained by extrapolation to $\delta m_\ell^{\mathrm{phys}}$ and then shifting by $\Delta X_{\mathrm{multiplet}}$, see the text. Two errors are displayed, showing the uncertainty with and without the error on $\Delta X_{\mathrm{multiplet}}$ included in quadrature.

to determine $\Delta X_{\mathrm{multiplet}}$ using the flavor averaged $J = \frac{1}{2}^+$ states and the corresponding experimental results. However, this would reduce predictability and the shift would still need to be estimated for the doubly charmed baryons. Instead we look for other multiplets that are likely to have similar $\Delta X_{\mathrm{multiplet}}$. Assuming that all the singly charmed multiplets are shifted by the same amount, we choose the flavor averaged light vector channel, $\frac{1}{3}(2M_{K^*} + M_\rho)$, to estimate $\Delta X_{\mathbf{6}} \approx \Delta X_{\bar{\mathbf{3}}}$. For the doubly charmed triplet we use the spin and flavor averaged heavy-light combination, $\frac{1}{12}(6M_{D^*} + 3M_{D_s^*} + 2M_D + M_{D_s})$. Treating the charm as a spectator, the D and D_s channels should form triplets and obey modified versions of Eqs. (13) and (14).

Figure 12 shows the light vector and D/D_s flavor singlet combinations as functions of M_π^2/X_π^2. As expected for quantities which depend on δm_ℓ to second order, there is very little change with the light quark mass. Note also that the extrapolation to $\delta m_\ell^{\mathrm{phys}}$ is relatively short. Fitting to a constant (fit 1) and a constant plus quadratic term (fit 2) we obtain extrapolated values, $M_{\mathrm{ave}} \pm \Delta M_{\mathrm{ave}}$, using the following formulae

$$M_{\mathrm{ave}} = \frac{1}{2}\left(\max_{i \in \{1, \dots n\}} (M_i + \Delta M_i) + \min_{i \in \{1, \cdots n\}} (M_i - \Delta M_i) \right), \tag{17}$$

$$\Delta M_{\mathrm{ave}} = \frac{1}{2}\left(\max_{i \in \{1, \dots n\}} (M_i + \Delta M_i) - \min_{i \in \{1, \cdots n\}} (M_i - \Delta M_i) \right), \tag{18}$$

where in this case $n = 2$, $M_i \pm \Delta M_i$ is the result from fit $i = 1, 2$. The difference of M_{ave} to experiment gives the estimate of $\Delta X_{\mathrm{multiplet}}$. ΔM_{ave} is taken as the error in the shift. For the D/D_s case the shift is consistent with zero, $-3(8)$ MeV, while for
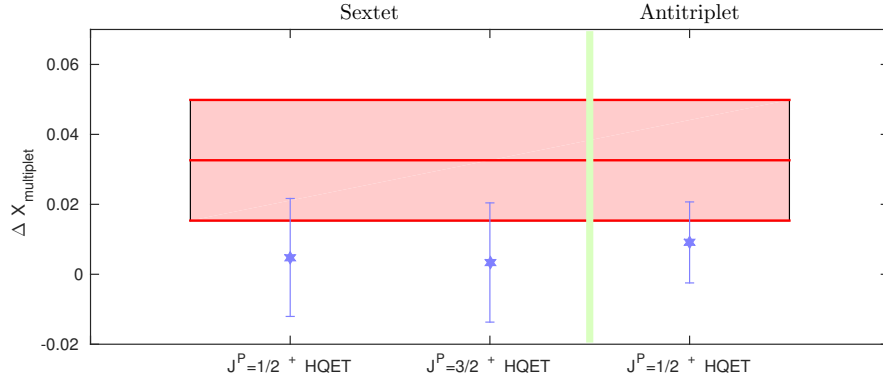
FIG. 13. The shift $\Delta X_{\mathrm{multiplet}}$ calculated by comparing different flavor averaged mass combinations with experiment both in the singly charmed sector (blue stars) and the light vector meson sector (shaded band).

the light vector it is $33(17)$ MeV.

Figure 12 also shows the positive parity charmed baryon flavor singlet combinations. Here, the data are extrapolated to $\delta m_{\ell}^{\mathrm{phys}}$ and the fit error is calculated as above. The appropriate shift, $\Delta X_{\mathrm{multiplet}}$ is applied, where the associated error is added in quadrature. Encouragingly, the final values are in agreement with experiment for the sextet and anti-triplet, consistent with $\Delta X_{\mathrm{multiplet}}$ being small and of a similar magnitude for the different multiplets. This is emphasized in Fig. 13 which compares $\Delta X_{\mathrm{multiplet}}$ determined from $\frac{1}{3}(2M_{K^*} + M_{\rho})$ with the shift obtained using the flavor averaged masses for the sextet and anti-triplet and the corresponding experimental values for the singly charmed baryons.

As for the mesons, there is very little dependence o δm_{ℓ} for all flavor average masses in Fig. 12. Ensembles on the correct trajectory, close to the physical point will be needed to quantify the size of the leading, i.e. $\mathrm{O}(\delta m_{\ell}^2)$, flavor symmetry violations. For our data the coefficients of the quadratic terms are zero within $2.5\,\sigma$.

C. Baryon and meson masses at the physical point

Turning to the extrapolation of the individual baryon masses our strategy is as follows. For a given multiplet, we employ the Gell-Mann–Okubo relations with and without the quadratic term, denoted GMO1 and GMO2, respectively. If the $\chi^2/\mathrm{dof} \lesssim 2$ for both fits, the final value for the mass at the physical point is computed using Eqs. (17) and (18) and performing the shift, $\Delta X_{\mathrm{multiplet}}$, as discussed above[8]. The mass values within a multiplet on a given ensemble are highly correlated. These correlations have been taken into account in the fits. Overall the GMO expressions describe the data well, however, in a small number of cases either the linear (GMO1) fit produced a $\chi^2/\mathrm{dof} > 2$ or both the linear and quadratic (GMO2) fits. If the masses do not fall into the GMO pattern, we can extrapolate using the functional forms Eqs. (10)–(16) but allowing the coefficients of the linear terms to differ for each member of a multiplet (i.e. only M_0 is constrained to be the same). Such phenomenological fits are always possible if $\overline{m}$ is kept fixed in the simulation. Again we considered these fits including and excluding quadratic terms, denoted as less-constrained 1 and 2 (LC1 and LC2), respectively. M_{ave} and ΔM_{ave} are calculated as above, where for the cases where we combined GMO2, LC1 and LC2 extrapolated results we take the minimum and maximum in Eqs. (17) and (18) of all three results[9]. Fig. 14 shows examples of the extrapolations. The corresponding values of the coefficients extracted from the fits are given in Table XIV (Appendix E). A summary of those fits included in the determination of the results at the physical point is provided in Table XI (Appendix E) and the final values are given in Table VII.

As mentioned above, the GMO expressions fit most data well, in particular the positive parity states. In the cases where the quadratic terms are statistically significant, the coefficients of these terms are generally small. The size of the linear and quadratic contributions at $\delta m_{\ell}^{\mathrm{phys}}$ are quantified in Fig. 15 for the ground state $J = \frac{1}{2}$ multiplets. The first order terms, for positive parity, are small while the second order terms are smaller still. For negative parity, both terms are reasonably small but of similar sizes. A larger set of ensembles with pion masses closer to the physical point are needed in order to reliably extract the coefficients and quantify the size of the individual terms. Interestingly, the $J^P = \frac{1}{2}^-$ anti-triplet (shown in Fig. 14) and the $J = \frac{3}{2}^-$ triplet could not be fitted to the GMO formulae. Indeed, Fig. 15 shows that for a quadratic fit the linear and quadratic contributions to the $J^P = \frac{1}{2}^-$ anti-triplet are both around $10 - 20\%$, albeit with large errors. This may indicate they have a more complicated

───────

[8] Whenever $\chi^2/\mathrm{dof} > 1$, the error $\Delta M_{1,2}$ is inflated by the factor $\sqrt{\chi^2/\mathrm{dof}}$.
[9] Note that for the LC2 fit there are as many data points as there are unknown coefficients, and thus there are no remaining degrees of freedom.

internal structure. We also remark that, as discussed in Section IV, our ground state spin-1/2 Ω_c and Ξ'_c negative parity results are likely to be scattering states. In the sextet, only the results for Σ_c away from the symmetric limit represent single particle states. From Fig. 14 we can see that a linear extrapolation to $\delta m_\ell^{\mathrm{phys}}$ of these two points would give consistent results with the GMO fit. The errors on the final values in Table VII are of similar sizes or larger than our estimate of the size of the discretization errors, in the range of $10 - 20$ MeV. Apart from the positive parity singly charmed baryons, the shift $\Delta X_{\mathrm{multiplet}}$ does not have a significant impact on the results.

Particle	Parity	M_1 (GeV)		M_2 (GeV)	
		SU(4)	HQET	SU(4)	HQET
Σ_c	$+$	2.414(13)(22)	2.434(20)(26)	3.090(94)(95)	3.144(115)(116)
Ξ'_c	$+$	2.534(09)(20)	2.543(12)(21)	3.177(67)(69)	3.226(72)(74)
Ω_c	$+$	2.642(07)(18)	2.648(09)(19)	3.268(47)(50)	3.294(50)(53)
Λ_c	$+$	2.280(15)(23)	2.280(17)(24)	3.183(75)(77)	3.181(76)(78)
Ξ_c	$+$	2.442(11)(21)	2.442(11)(20)	3.234(37)(41)	3.245(36)(40)
Ξ_{cc}	$+$	3.610(09)(12)	3.610(09)(12)	4.017(39)(40)	4.018(40)(41)
Ω_{cc}	$+$	3.713(06)(10)	3.713(06)(10)	4.157(31)(32)	4.158(31)(32)
Σ_c^*	$+$		2.506(18)(25)		3.234(121)(122)
Ξ_c^*	$+$		2.608(13)(22)		3.295(87)(89)
Ω_c^*	$+$		2.709(11)(21)		3.355(64)(66)
Ξ_{cc}^*	$+$		3.694(07)(11)		4.078(36)(37)
Ω_{cc}^*	$+$		3.785(06)(10)		4.215(26)(28)
Σ_c	$-$	2.698(87)(89)			
Ξ'_c	$-$	2.850(44)(47)**			
Ω_c	$-$	2.995(20)(26)**			
Λ_c	$-$		2.578(144)(145)		
Ξ_c	$-$		2.761(77)(79)		
Ξ_{cc}	$-$		3.892(47)(48)	4.306(45)(44)	
Ω_{cc}	$-$		4.061(28)(29)	4.394(42)(41)	
Σ_c^*	$-$		2.740(48)(51)		
Ξ_c^*	$-$		2.891(32)(36)		
Ω_c^*	$-$		3.016(32)(37)		
Ξ_{cc}^*	$-$		3.989(58)(58)		4.447(57)(57)
Ω_{cc}^*	$-$		4.132(42)(43)		4.567(55)(56)

TABLE VII. Mass estimates at the physical point for the ground and first excited states of the singly and doubly charmed positive and negative parity baryons. The mean is computed using Eq. (17) for the fits indicated in Table XI and includes the shifts $\Delta X_{\mathrm{multiplet}}$. The first error is due to varying the fit parameterization and is calculated using Eq. (18), while the second error includes the uncertainty associated with $\Delta X_{\mathrm{multiplet}}$. Note that for the negative parity channels we only give results for the operators for which the mass could reliably be extracted. The superscript ** indentifies likely scattering states. The results for the first excitations may also contain such states.

Finally, we present the extrapolations for the mesons. The charmonium channels are fitted individually as for the other flavor singlets discussed above (to a constant and a constant plus quadratic term). Figure 16 displays the extrapolations for the heavy-light mesons, Table XII (Appendix E) details the fit functions used. Since the heavy-light mesons form triplets, the expressions Eqs. (13) and (14) apply. While the lowest lying 0^- and 1^- states exhibit GMO dependence on δm_ℓ, this does not hold for the higher states. In particular, in the 0^+ channel, the lowest eigenvalue for the $\bar{c}\ell$ interpolator decreases rapidly towards $\delta m_\ell^{\mathrm{phys}}$ and is very close in value to the corresponding non-interacting $D\pi$ state on each ensemble. In contrast, replacing the light quark with a strange quark, the D_{s0}^* is below DK and is consistent with experiment at the physical point. Unfortunately, we were not able to reliably extract higher eigenvalues in these channels, nor did expanding the interpolator basis to include $\bar{c}\gamma_4 q$ prove successful. Further work, including interpolators with derivatives will be performed in the future. A similar picture emerges for the 1^+, however, here we are able to resolve closely lying levels by using two interpolators (see Table II). For the D meson case, the lowest eigenvalue coincides with $D^*\pi$, while the next level is much less sensitive to the light quark mass and is compatible with experiment at the physical point, leading us to associate this level with the D_1. Switching to the D_s sector, the lowest level is below the D^*K threshold and is consistent with the $D_{s1}(2460)$. The next level is both consistent with D^*K and with $D_{s1}(2536)$. A careful finite volume study is needed to clarify this issue.
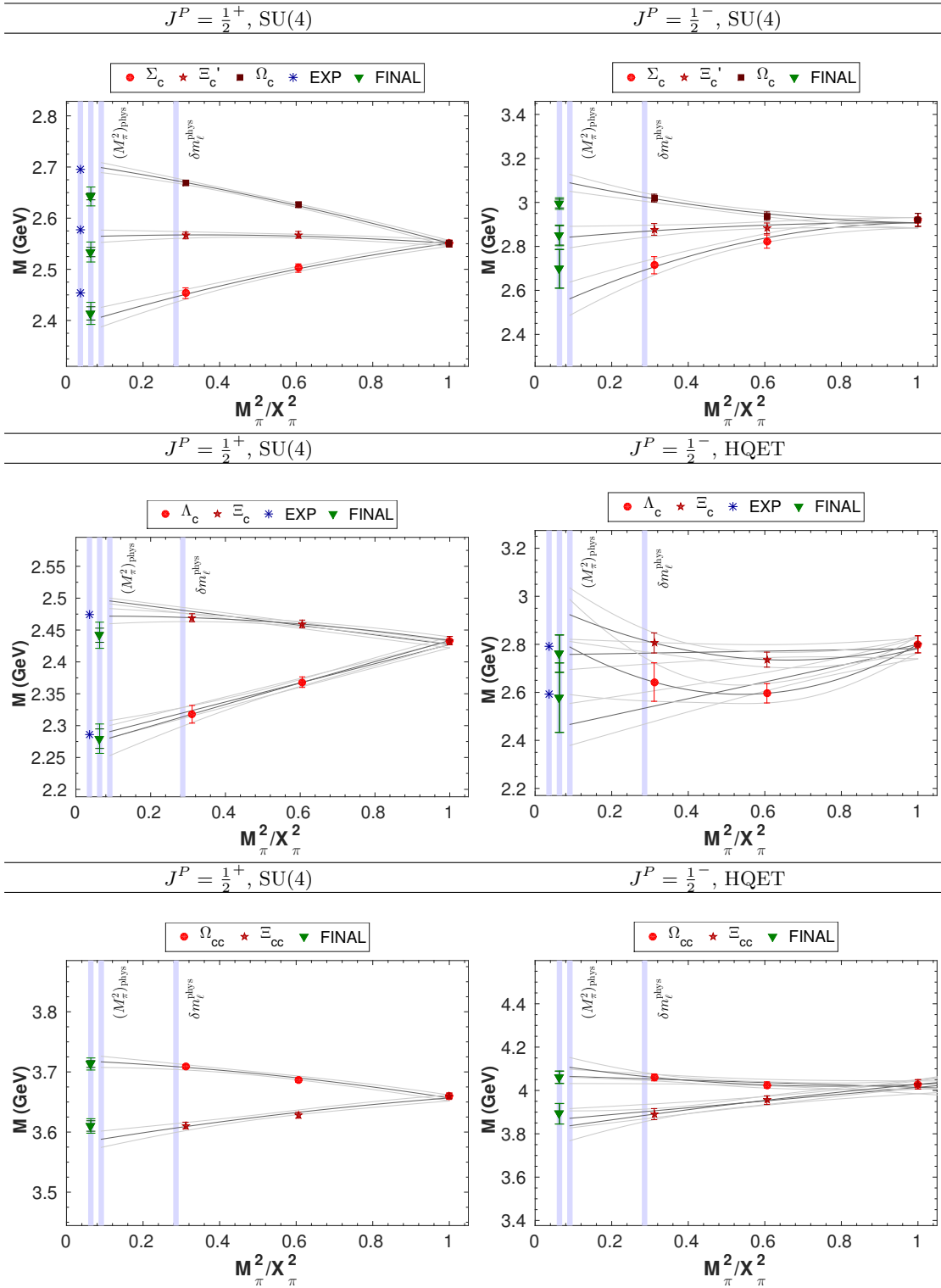
FIG. 14. Extrapolation to $\delta m_\ell^{\mathrm{phys}}$ for (left) positive parity and (right) negative parity charmed baryons on $V = 32^3 \times 64$ ensembles. The final (extrapolated) results are displayed as in Fig. 12, with the shift $\Delta X_{\mathrm{multiplet}}$ included. The type of fit displayed (GMO or LC) corresponds to that used to determine the final values, see Table XI. For improved visibility, where GMO2, LC1 and LC2 fits were used, we only show the GMO2 fit. The type of interpolators chosen for each multiplet (HQET/SU(4)) is given above each plot. Where available the experimental results are displayed on the very left.
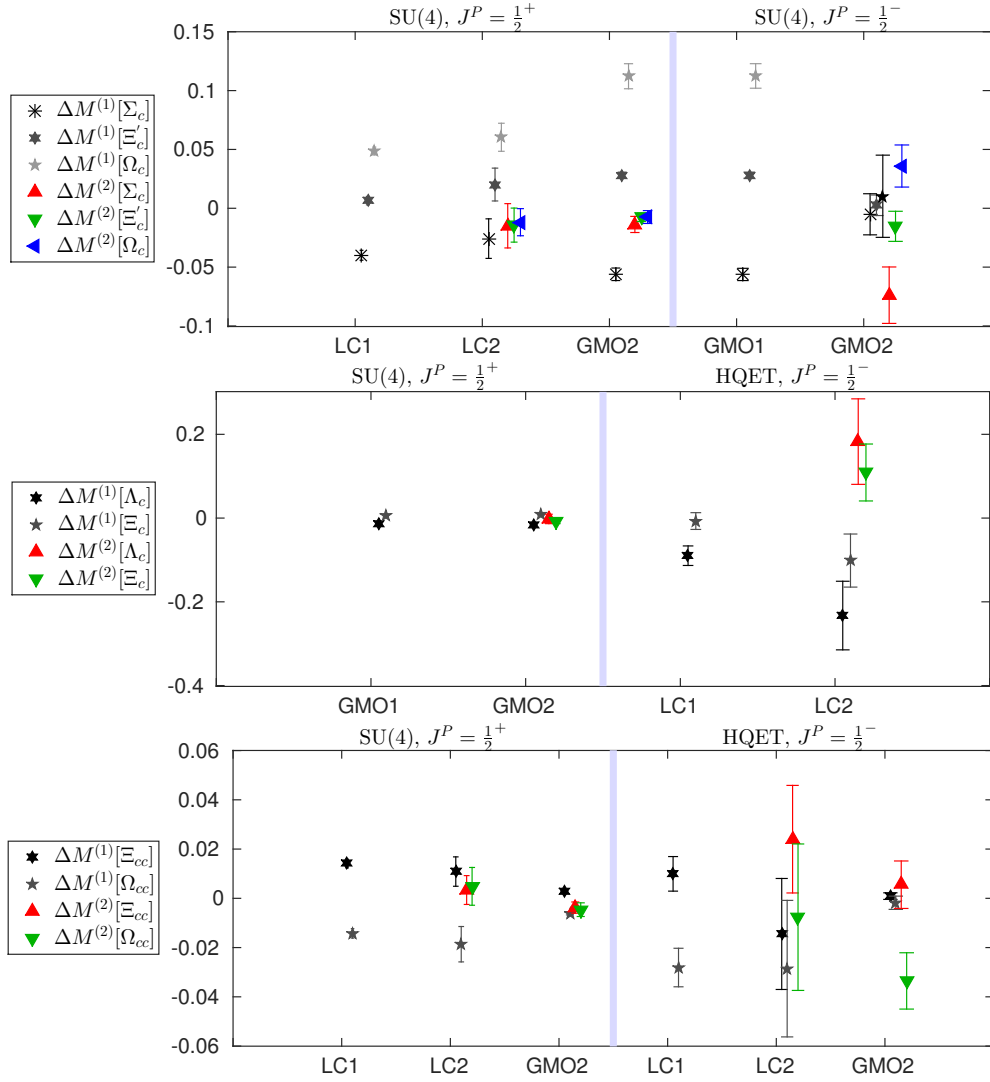
FIG. 15. Contributions of the first and second order terms in the expansions in δm_ℓ evaluated at $\delta m_\ell^{\text{phys}}$ for each multiplet displayed in Fig. 14. The contributions are given as a percentage of the baryon mass of each multiplet in the SU(3) flavour limit (M_0), i.e. $M_B = M_0(1 + \Delta M^{(1)} + \Delta M^{(2)})$ for each baryon mass M_B.

D. Mass differences

Mass differences uncover specific aspects of the quark dynamics within the charmed baryons. We focus on three types of positive parity ground state mass differences, spin $(J = \frac{3}{2}) - (J = \frac{1}{2})$, "structure" (between the sextet and anti-triplet multiplets) and flavor (within multiplets corresponding to changing $s \to u/d$ and between multiplets for $c \to u/d$ and $c \to s$). The splittings are computed from the jackknifes of the individual masses and are extrapolated to $\delta m_\ell^{\text{phys}}$ using functional forms derived by taking the differences of the expressions for the masses. The parameterizations used for each channel are listed in Table XIII. With the assumption that the singly charmed multiplets all require shifts, $\Delta X_{\text{multiplet}}$, of a similar size to make contact with the physical point, only the $c \to u/d$ and $c \to s$ flavor splittings require a correction. The final results are displayed in Fig. 17.

- **Spin splittings:** according to the predictions of HQET/pNRQCD, the $\frac{3}{2} - \frac{1}{2}$ mass differences should be small, of $O(\overline{\Lambda}^2/m_c)$, vanishing in the static limit. Figure 17 shows all spin splittings are indeed small, in the region of 60–85 MeV. They are also similar in size, independent of the light quark content and the number of charm quarks. This can be understood as follows. For doubly charmed baryons, if the two charm quarks form a spatially small diquark ($r \ll \overline{\Lambda}^{-1}$), the spin difference should correspond to 3/4 times the corresponding D (or D_s) fine structure splitting, where a factor $3/2$ is from coupling a $s_d = 1$ or $s_d = 0$ diquark, rather than a spin-1/2 antiquark, to the light quark. Another factor
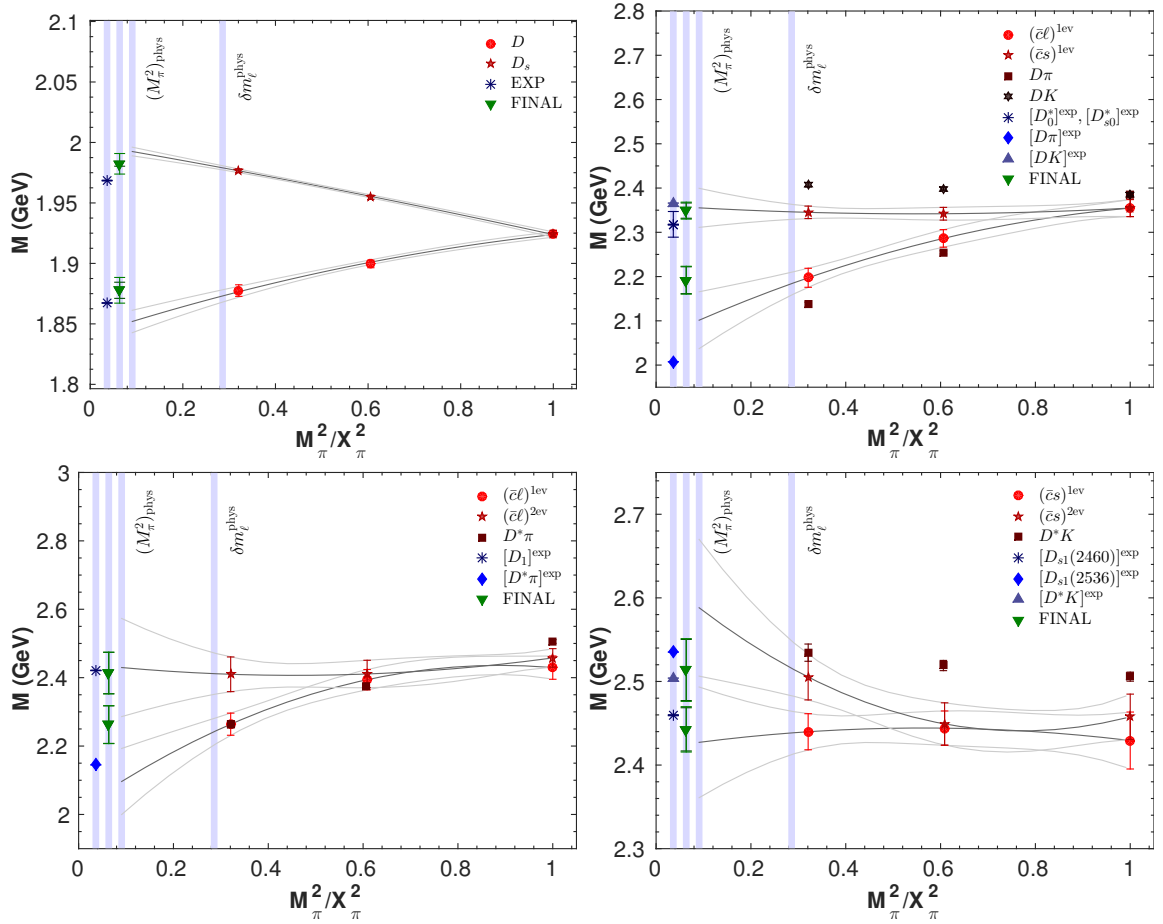
FIG. 16. Extrapolations to the physical point for (top left) the D and D_s mesons, (top right) the D_0^* and D_{s0}^* mesons, (bottom left) the lowest two eigenvalues for D_1 and (bottom right) the lowest two eigenvalues for D_{s1}. For simplicity one fit is displayed in each case. The full set of fits used to calculate the final values are given in Table XII (Appendix E). These values include the shift $X_{\text{multiplet}}$ (and corresponding error) determined from the spin and flavor averaged D/D_s mass. For the D_0^*, D_1 and D_{s1} the results for the relevant non-interacting two particle states are also shown.

$1/2$ is due to the different color contraction within a baryon, relative to the meson color trace [63][10]. Testing this HQET picture (or, equivalently, the short-distance pNRQCD picture), we have $\frac{3}{4}(M_{D^*} - M_D) = 95(8)$ MeV compared to $M_{\Xi_{cc}^*} - M_{\Xi_{cc}} = 85(9)$ MeV and $\frac{3}{4}(M_{D_s^*} - M_{D_s}) = 92(2)$ MeV compared to $M_{\Omega_{cc}^*} - M_{\Omega_{cc}} = 71(4)$ MeV. The Ω_{cc} splitting agrees less well with this expectation, however, higher order corrections in HQET and (p)NRQCD of size $\overline{\Lambda}^3/m_c^2$ and $m_c v^6$, respectively, are not necessarily small at the charm quark mass. Brown et al. [43], making a similar comparison (using the experimental meson splittings), find that agreement improves for bottom quarks. We remark that singly charmed baryons, where the two light quarks form a diquark, share the same spin- and color-factors of doubly charmed baryons ($\frac{3}{2} \cdot \frac{1}{2} = \frac{3}{4}$), relative to charmed mesons. Therefore, also the Σ_c, Ξ_c and Ω_c fine structure splittings are of similar sizes, see Fig. 17. Finally, for $r > \overline{\Lambda}^{-1}$, doubly charmed baryons become similar to charmonia. Again, the spin and color factors are the same but in this case one should compare to the charmonium fine structure, $\frac{3}{4}(M_{J/\psi} - M_{\eta_c}) = 76(1)$ MeV. The situation is now reversed with the Ω_{cc} splitting being in closer agreement. Therefore, based on the fine structure, it is not possible to cleanly discriminate between the two cases (HQET or charmonium-like). As discussed in Section II, from the meson sector we expect discretization effects in spin splittings of about 10–20 MeV, while the final errors in the figure are around 5–10 MeV. Nevertheless the sextet differences are reasonably consistent with experiment.

- **Flavor structure splittings**: these are differences between baryons with the same J^P and quark content but different flavor structure. The Λ_c ($I = 0$) and Σ_c ($I = 1$) lie in the anti-triplet and sextet multiplets, respectively, and differ in

---

[10] In pNRQCD this factor is due to the light quark interacting with two color charges, in HQET one would ascribe it to the mass of an effective $\overline{Q} = cc$ antiquark.
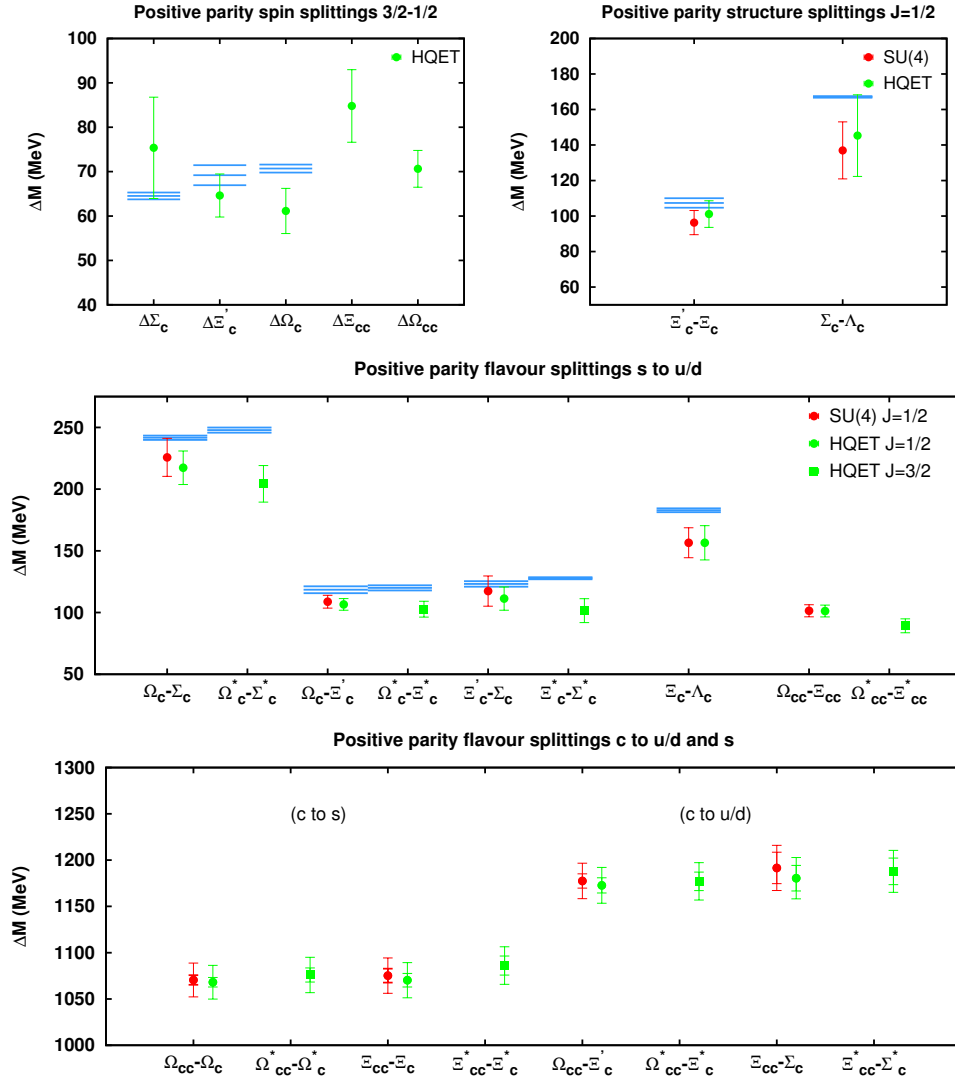
FIG. 17. The spin and flavor mass splittings for the positive parity charmed baryons on the $V = 32^3 \times 64$ ensembles. For the splittings where the charm quark is replaced by a strange or light quark (bottom plot) two errors are shown indicating the uncertainty with and without the error on $\Delta X_{\mathrm{multiplet}}$; this shift cancels in the other splittings. The experimental values are indicated, where we take the J^P assignment suggested by the PDG in the cases where the quantum numbers have not been identified. The experimental errors are shown as bands. For those splittings for which a value is not quoted by the PDG, the error is calculated adding the uncertainties of the individual masses in quadrature.

isospin. Similarly, the Ξ'_c and the Ξ_c share the same valence quark content but differ in terms of their SU(3) wavefunctions. Nature respects isospin symmetry reasonably well but not so SU(3); the physical Ξ'_c and Ξ_c states may be mixtures of the sextet and the anti-triplet states. While we have not studied this mixing we note that Brown et al. [43] found that such effects are not significant. In Fig. 17 one can see that the splittings are compatible with experiment.

- **Flavor splittings**: in the middle panel of Fig. 17 we show differences between masses of particles where one or two strange quarks are replaced by light quarks. The mass differences for $ss \to \ell\ell$ are roughly twice as large as those for $s \to \ell$. Agreement is found with experiment for differences involving $J = \frac{1}{2}$ singly charmed baryons, however, our results seem to be systematically (slightly) lower for $J = \frac{3}{2}$. In the last panel of Fig. 17 we show differences between masses of doubly charmed baryons and their singly charmed counterparts, replacing either one charm quark by a strange quark or by an up/down quark. Clearly, $M_{\Omega^*_{cc}} - M_{\Omega^*_c} \approx M_{\Omega_{cc}} - M_{\Omega_c}$ since $M_{\Omega^*_{cc}} - M_{\Omega_{cc}} \approx M_{\Omega^*_c} - M_{\Omega_c}$ etc., as already observed above under "Spin splittings". However, also $M_{\Omega_{cc}} - M_{\Omega_c} \approx M_{\Xi_{cc}} - M_{\Xi_c}$ and $M_{\Omega_{cc}} - M_{\Xi'_c} \approx M_{\Xi_{cc}} - M_{\Sigma_c}$, suggesting the dynamics of doubly charmed baryons to be closely linked to those of singly charmed baryons (and charmed mesons); in the first case the two heavy quarks seem to form a diquark (meaning $r \ll \overline{\Lambda}^{-1}$) while in the second case either the light quarks form a diquark, interacting with the remaining charm quark or one light quark interacts with a heavy-light core. This would explain why the two systems resemble each other closely, up to constant shifts, due to differences of

the respective (constituent) quark masses. Note that replacing the remaining charm quark by a light quark flavor will not result in constant energy shifts. For example, the fine structure of the light and heavy baryons are very different.

E. Comparison with previous results

Our final results for the individual masses are summarized in Fig. 18, where for the negative parity channels only the results for interpolators which gave a reliable signal are shown. Overall, for the singly charmed baryons there is reasonable agreement with experiment, as also seen for the mesons with open and hidden charm, which is encouraging in terms of the size of the remaining systematics. In particular, in some previous calculations $M_{cqq} - \frac{1}{2}M_{\eta_c}$ or $M_{ccq} - M_{\eta_c}$ splittings were computed, instead of the individual baryon masses, in order to remove the dependence on the charm quark mass and to reduce the size of discretization effects and uncertainties arising from tuning the charm quark mass using the meson sector. This has not been done here. However, states involving strange quarks are systematically lower than experiment, in particular, the Ω_c. This may be due to residual effects related to simulating along an incorrect $\overline{m} = \mathrm{constant}$ line. Furthermore, our finite volume study suggests that the positive parity ground state singly charmed baryons and excited state doubly charmed baryons will decrease by a few tens of MeV in the infinite volume limit.
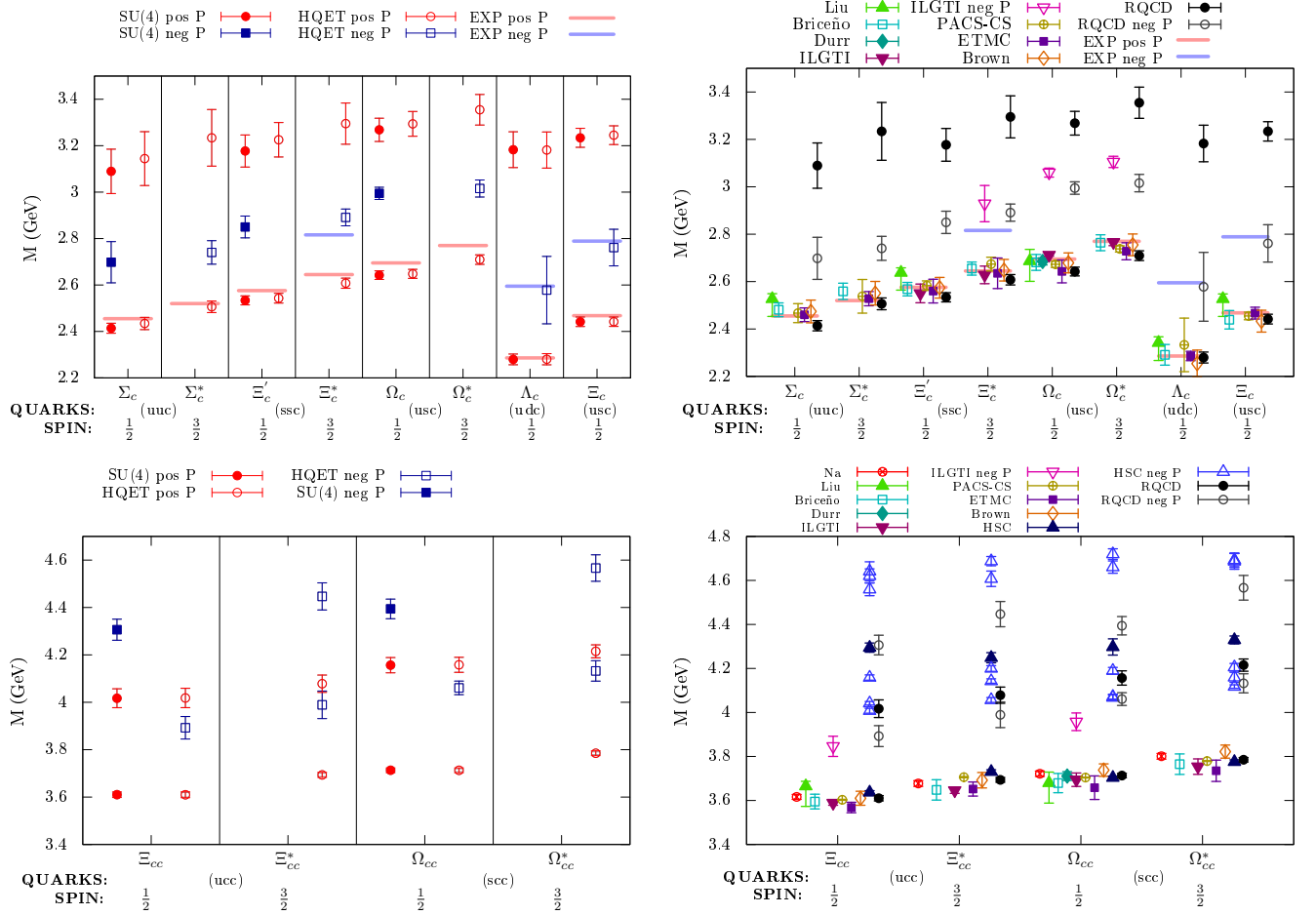

FIG. 18. Singly charmed (top) and doubly charmed (bottom) low lying baryon spectra. (Left) our results (RQCD) from the $V = 32^3 \times 64$ ensembles. (Right) a comparison with previous determinations from Na et al. [35], Liu et al. [36], Briceño et al. [37], Dürr et al. [40], ILGTI [39], PACS-CS collaboration [41], ETMC [42], Brown et al. [43] and HSC [44]. Note that our results for the negative parity, spin-1/2 Ω_c and Ξ'_c are likely scattering states, see Section IV. The first excitations may also contain such states.

There have been a number of recent lattice studies of the charmed baryon spectra, also displayed in Fig. 18, most of which are restricted to positive parity ground states. Different systematics apply in each case depending on,

- the number of sea quarks included: $N_f = 2$ (Dürr et al. [40]), $N_f = 2 + 1$ (Na et al. [35], Liu et al. [36], PACS-CS [41], Brown et al. [43], HSC [44]) and $N_f = 2 + 1 + 1$ (Briceño et al. [37], ILGTI [39], ETMC [42]).

- The charm quark action: the Fermilab action [73] (Na et al., Liu et al.), a relativistic heavy quark action [74, 75] (Briceño et al., PACS-CS, Brown et al.), twisted mass [76] (ETMC), anisotropic clover [77] (HSC), the Brillouin action [40] (Dürr et al.) and the overlap action [78] (ILGTI).

- The light valence and sea quark action: MILC Asqtad staggered sea [79] and valence (Na et al.), MILC Asqtad staggered sea [79] with domain wall valence (Liu et al.), MILC HISQ sea [80] with tadpole-improved clover valence (Briceño et al.), QCDSF non-perturbative clover sea [81] with Brillouin valence (Dürr et al.), MILC HISQ sea [80] with overlap valence (ILGTI), non-perturbative clover sea [82] and valence (PACS-CS), twisted mass sea [42] and valence (ETMC), RBC/UKQCD domain wall sea [83] and valence (Brown et al.) and anisotropic tadpole-improved clover sea [44] and valence (HSC).

Systematics arise from finite lattice spacings, unphysical quark masses, finite volumes, excited state contamination and, among mixed action approaches, violations of unitarity. Notable are the Briceño et al. [37], ETMC [42] and Brown et al. [43] studies, involving both continuum and chiral limit extrapolations, the other works are predominately at a single lattice spacing. Despite such varied approaches, there is general agreement for the spectra. In particular, the lattice results are approximately 80 MeV above the SELEX measurement of $M_{\Xi_{cc}} = 3518.7(1.7)$ [12]. The recent result of Borsanyi et al., $M_{\Xi_{cc}^{++}} - M_{\Xi_{cc}^+} = 2.16(11)(17)$ MeV [84] also contradicts the SELEX value of approximately 60 MeV for this isospin splitting [13].

Of particular interest for our work are the determinations of ground state negative parity particles by ILGTI [39] and the ground state and excitations for both parities for the doubly charmed spectrum by HSC [44]. ILGTI use pion masses down to 240 MeV and two lattice spacings, $a = 0.06$ fm and 0.09 fm, both with a spatial extent $L = 2.9$ fm while HSC employ a temporal lattice spacing of $a_t \sim 0.035$ fm on anisotropic lattices with $L = 1.9$ fm and a single pion mass, $M_\pi = 391$ MeV. Considering the different systematics involved in each study, Fig. 18 shows that the determinations for the ground state negative parity channels are reasonably consistent, including those which we identify as scattering states. The picture is less satisfying comparing with the HSC predictions for excited doubly charmed baryons. Our positive parity first excited states are significantly below those of HSC[11], even for the $\Omega_{cc}^{(*)}$. This may be due to finite volume effects and/or the lack of chiral extrapolation in the HSC study. Certainly the discrepancy is smaller for the $\Omega_{cc}^{(*)}$ compared to the $\Xi_{cc}^{(*)}$ and, as discussed in Section VI A, we expect finite volume effects to increase the mass for smaller physical volumes. For the negative parity states, HSC predict several levels (as expected from non-relativistic quark models with SU(6)×O(3) symmetry, see Ref. [44] for a discussion) in the range $4.0 - 4.8$ GeV. With only one interpolator (but multiple smearings) we are not able to resolve closely lying states and our excited states are above the first three HSC levels. With our limited basis the first excitation could also have an overlap with a state corresponding to higher continuum spin. This would correspond to $J = \frac{7}{2}$ for spin-1/2 interpolators and $J = \frac{5}{2}$ for spin-3/2. A more extensive analysis is needed in order to make a closer comparison.

VII. CONCLUSIONS

In this work we have presented results for the ground states and first excitations of singly and doubly charmed baryons. Through the use of the variational method with a basis of three differently smeared interpolators, reliable signals were obtained for both positive and negative parities, where for the latter the first excitation was only extracted for doubly charmed states. For spin-1/2 channels we implemented both HQET and SU(4) inspired interpolators and found consistent results for positive parities, while for negative parities SU(4) interpolators had a much better overlap with the ground state for sextet baryons ($\Sigma_c, \Xi_c', \Omega_c$) and HQET interpolators for the anti-triplet (Λ_c, Ξ_c) and triplet (Ξ_{cc}, Ω_{cc}). Overall agreement was obtained with experiment, where available, suggesting the remaining systematics are not large. This is supported by the results for the lower lying charmonium, D and D_s mesons, which also reproduced the gross experimental spectra. Discretization effects can be significant in a simulation at a single lattice spacing, for which $am_c \sim 0.4$. Fine structure is particularly sensitive to such effects, and in the meson sector spin splittings were underestimated by 10–20 MeV. However, for the singly charmed baryons the spin splittings are consistent with experiment within statistical uncertainties ranging from 5 to 11 MeV. Our study of finite volume effects suggests the lightest members of the ground state singly charmed multiplets and first excitations of the doubly charmed triplet, in the infinite volume limit, could be around 1σ lower (in terms of the final quoted error).

The negative parity channels and first excitations of both parities require careful study due to a number of decay channels with thresholds close to our mass estimates. By looking for degeneracy of the masses with the threshold values on each ensemble, over the range of pion masses $M_\pi = 259 - 461$ MeV, we identified the ground states in the Ω_c and Ξ_c' negative parity channels as scattering states. Interestingly, for the singly charmed anti-triplet the HQET interpolators had a good overlap with the level consistent with a bound state, while the SU(4) interpolators gave results consistent with the corresponding thresholds. We

---

[11] For improved visibility we have omitted the HSC results for positive parity higher excitations from Fig. 18.

also encountered scattering states in the meson spectra, where, by including additional interpolators in the variational basis, results consistent with experiment for the D_1 and D_{s1} were obtained. Cross-correlation functions between the SU(4) and HQET interpolators would be needed to repeat this analysis for the baryons.

One of the main aims of our study was to investigate the light flavor structure of charmed baryons: employing ensembles with the average light quark mass fixed enables expansions in the flavor symmetry breaking quark mass difference, starting from a point where the lattice results are most precise. The corresponding Gell-Mann–Okubo relations worked well for almost all multiplets and the extrapolations were well constrained, with the linear terms in δm_ℓ within each multiplet being fixed by one coefficient. In some cases the quadratic terms were statistically significant, however, the magnitudes of these contributions were still small. A notable exception was the singly charmed anti-triplet (Λ_c, Ξ_c), which did not fit the GMO pattern. This may indicate a more complex internal structure. However, one can still perform a phenomenological fit using an expansion in δm_ℓ, where the linear coefficients are not constrained. The errors on our final values were estimated conservatively, including both linear and quadratic fits. An additional uncertainty is present in our results due to the simulation trajectory missing the physical point in the mass plane. This effect was corrected for in a consistent way and the agreement found with experiment for extrapolated flavor singlet mass combinations suggests the correction is small. However, we note that our results for heavy baryons involving strange quarks are consistently lower than experiment which may indicate residual effects.

The dynamics of quarks within heavy baryons is interesting in terms of possible similarities with the heavy-heavy or heavy-light mesons and the applicability of various effective theories. In particular, for doubly charmed baryons, there are two relevant limits, in terms of a point-like heavy-heavy diquark (the HQET or short distance pNRQCD picture) or a more diffuse heavy-light diquark (charmonium picture). Flavor splittings where the charm quark is replaced by a strange or up/down quark suggest the dynamics of doubly charmed baryons are closely linked to those of singly charmed ones.

In the future we plan to perform a more extensive study on CLS configurations [50], with a larger range of pion masses, all with $LM_\pi \gtrsim 4$. This will enable a further investigation of the magnitude of flavor symmetry breaking effects. Initial studies show the physical trajectory has been reproduced reasonably well [85].

Appendix A: Meson effective masses

Effective masses of the lowest two eigenvalues for a number of channels for charmonium and D/D_s are shown in Fig. 19 for the larger symmetric ensemble. The effective masses for the lowest four eigenvalues for D_1 and D_{s1} on the $M_\pi = 259$ MeV ensemble are displayed in Fig. 20.
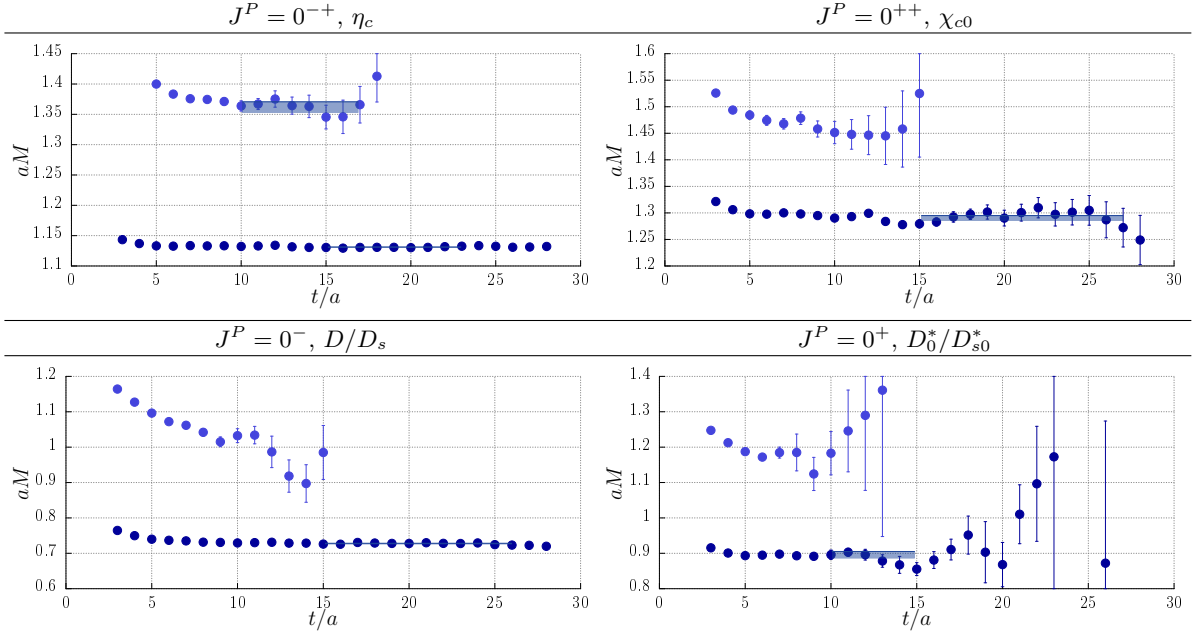

FIG. 19. Sample of effective masses of the charmonium and D/D_s mesons for the symmetric ensemble with $V = 32^3 \times 64$. The filled regions indicate the fitting ranges chosen and the fit result including errors.
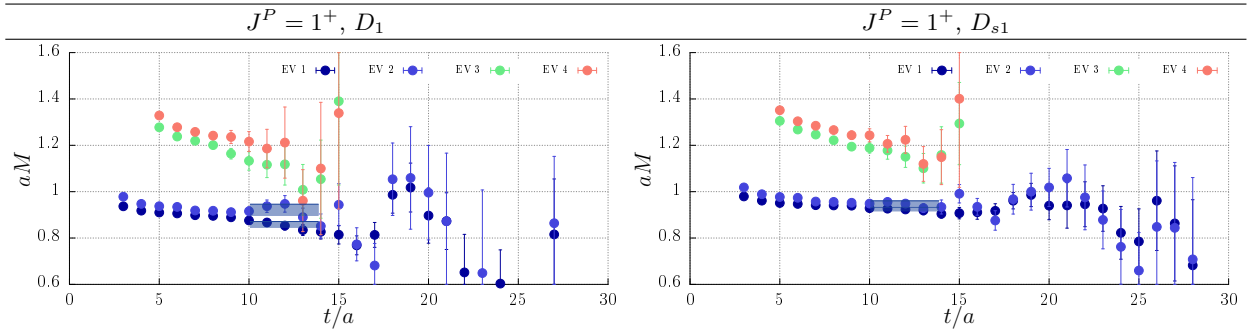

FIG. 20. As in Fig. 19 for the effective masses of the lowest four eigenvalues (EV) for the 1^+ channels on the $M_\pi = 259$ MeV ensemble with $V = 32^3 \times 64$.

Appendix B: Finite volume effects

The finite volume effects computed using the matched $V = 24^3 \times 48$ and $32^3 \times 64$ ensembles are given in Tables VIII and IX for positive and negative parity particles, respectively.

Particle	P		First eigenvalue				Second eigenvalue			
			SU(4)		HQET		SU(4)		HQET	
			ΔM (MeV)	$\frac{\Delta M}{M_{32}}$ (%)	ΔM (MeV)	$\frac{\Delta M}{M_{32}}$ (%)	ΔM (MeV)	$\frac{\Delta M}{M_{32}}$ (%)	ΔM (MeV)	$\frac{\Delta M}{M_{32}}$ (%)
$\Sigma_c, \Xi'_c, \Omega_c$	+	κ_{sym}	33(10)	1.3	24(11)	0.9	-63(89)	-1.9	-59(81)	-1.8
Σ_c	+		31(15)	1.2	15(16)	0.6	69(134)	2.1	-4(139)	-0.1
Ξ'_c	+	κ_{asym}	18(11)	0.7	16(11)	0.6	50(102)	1.5	-19(96)	-0.6
Ω_c	+		10(8)	0.4	8(9)	0.3	31(84)	1.0	-22(77)	-0.7
$\Sigma^*_c, \Xi^*_c, \Omega^*_c$	+	κ_{sym}			39(12)	1.5			-139(90)	-4.0
Σ^*_c	+				27(17)	1.0			129(164)	3.8
Ξ^*_c	+	κ_{asym}			15(12)	0.6			67(108)	2.0
Ω^*_c	+				6(10)	0.2			34(84)	1.0
Λ_c, Ξ_c	+	κ_{sym}	32(8)	1.3	33(8)	1.4	-229(98)	-7.0	-266(98)	-8.1
Λ_c	+	κ_{asym}	19(12)	0.8	20(13)	0.9	-139(187)	-4.4	-150(201)	-4.7
Ξ_c	+		11(9)	0.5	12(9)	0.5	-63(121)	-1.9	-72(126)	-2.2
Ω_{cc}, Ξ_{cc}	+	κ_{sym}	4(6)	0.1	3(6)	0.1	76(24)	1.9	79(24)	1.9
Ξ_{cc}	+	κ_{asym}	4(8)	0.1	6(7)	0.2	63(29)	1.5	56(29)	1.4
Ω_{cc}	+		-1(6)	-0.0	0(5)	0.0	43(27)	1.0	39(27)	0.9
$\Omega^*_{cc}, \Xi^*_{cc}$	+	κ_{sym}			9(7)	0.3			87(26)	2.1
Ξ^*_{cc}	+	κ_{asym}			1(9)	0.0			69(30)	1.7
Ω^*_{cc}	+				-5(7)	-0.1			46(27)	1.1

TABLE VIII. Mass differences, $\Delta M = M_{24} - M_{32}$, between the positive parity masses extracted from the $V = 24^3 \times 48$ and the $32^3 \times 64$ ensembles, where the quark mass parameters (κ) are the same: the symmetric point $\kappa_{\mathrm{sym}} = 0.1209$ and the asymmetric combination $\kappa_{\mathrm{asym}} = (0.12104, 0.12062)$. The errors on the differences are computed by adding the individual uncertainties in quadrature.

Particle	P		Operator	ΔM (MeV)	$\frac{\Delta M}{M_{32}}$ (%)
First eigenvalue					
$\Sigma_c, \Xi'_c, \Omega_c$	-	κ_{sym}	SU(4)	-36(37)	-1.2
Σ_c	-			-49(40)	-1.7
Ξ'_c	-	κ_{asym}	SU(4)	-37(31)	-1.3
Ω_c	-			-22(24)	-0.7
Λ_c, Ξ_c	-	κ_{sym}	HQET	-4(40)	-0.1
Λ_c	-	κ_{asym}	HQET	122(48)	4.7
Ξ_c	-			63(36)	2.3
Ω_{cc}, Ξ_{cc}	-	κ_{sym}	HQET	9(23)	0.2
Ξ_{cc}	-	κ_{asym}	HQET	-2(23)	-0.1
Ω_{cc}	-			-8(17)	-0.2
$\Omega^*_{cc}, \Xi^*_{cc}$	-	κ_{sym}	HQET	-19(23)	-0.5
Ξ^*_{cc}	-	κ_{asym}	HQET	-39(22)	-1.0
Ω^*_{cc}	-			-31(16)	-0.8
Second eigenvalue					
Ω_{cc}, Ξ_{cc}	-	κ_{sym}	SU(4)	22(47)	0.5
Ξ_{cc}	-	κ_{asym}	SU(4)	43(46)	1.0
Ω_{cc}	-			32(39)	0.7
$\Omega^*_{cc}, \Xi^*_{cc}$	-	κ_{sym}	HQET	-67(39)	-1.5
Ξ^*_{cc}	-	κ_{asym}	HQET	79(52)	1.8
Ω^*_{cc}	-			21(36)	0.5

TABLE IX. As in Table VIII for the negative parity states.

Tensor	rank	Representation
S	$(0,0)$	**1**
q^a	$(1,0)$	**3**
q_a	$(0,1)$	$\overline{\mathbf{3}}$
O_b^a	$(1,1)$	**8**
S^{ab}	$(2,0)$	**6**
S_{ab}	$(0,2)$	$\overline{\mathbf{6}}$
D^{abc}	$(3,0)$	**10**
D_{abc}	$(0,3)$	$\overline{\mathbf{10}}$
T_{ab}^{cd}	$(2,2)$	**27**

TABLE X. Tensors corresponding to the lower dimensional irreducible representations of SU(3).

Appendix C: Tensorial notation for SU(3) representations

For convenience we review the tensor notation for SU(3) representations. Consider a general SU(3) tensor $T_{b_1 \ldots b_m}^{a_1 \ldots a_n}$ with n contravariant indices and m covariant indices (i.e. rank (n, m)), which transforms according to

$$T_{b_1 \ldots b_m}^{a_1 \ldots a_n} \to U_{a_1}^{a_1'} \ldots U_{a_n}^{a_n'} T_{b_1 \ldots b_m}^{a_1 \ldots a_n} (U^\dagger)_{b_1'}^{b_1} \ldots (U^\dagger)_{b_n'}^{b_n}, \tag{C1}$$

where U is the SU(3) transformation. We can construct lower rank tensors starting from $T_{b_1 \ldots b_m}^{a_1 \ldots a_n}$ by performing the following contractions,

$$
\begin{aligned}
\delta_{a_i}^{b_j} T_{b_1 \ldots b_m}^{a_1 \ldots a_n}, \quad &\text{for} \quad 1 \le i \le n, 1 \le j \le m, \quad \text{rank } (n-1, m-1), \\
\epsilon_{a_i a_j b_{m+1}} T_{b_1 \ldots b_m}^{a_1 \ldots a_n} \quad &\text{for} \quad 1 \le i, j \le n, \quad \text{rank } (n-2, m+1), \\
\epsilon^{b_i b_j a_{n+1}} T_{b_1 \ldots b_m}^{a_1 \ldots a_n} \quad &\text{for} \quad 1 \le i, j \le m, \quad \text{rank } (n+1, m-2),
\end{aligned}
\tag{C2}
$$

where δ_a^b, ϵ_{abc} and ϵ^{abc} are SU(3) invariant. Irreducible tensors cannot be expressed in terms of tensors of lower rank, and hence, one obtains zero from any of the above contractions. This means that the irreducible tensors are pairwise symmetric in both the covariant and contravariant indices and traceless on any index. The lower dimensional irreducible tensors are listed in Table X, with the dimension $D(m, n) = \frac{1}{2}(n+1)(m+1)(n+m+2)$. We are interested in decomposing the product of two irreducible representations. The tensor product is expressed in terms of the irreducible tensors and δ_a^b, ϵ_{abc} or ϵ^{abc}. For example,

$$\mathbf{3} \otimes \overline{\mathbf{3}} = \mathbf{1} \oplus \mathbf{8}, \quad q^a q_b = \frac{1}{3} \delta_b^a S + O_b^a. \tag{C3}$$

Similarly, tensors of irreducible representations can be expressed in terms of the components of the fundamental representation,

$$S = q^c q_c \text{ and } \quad O_b^a = q^a q_b - \frac{1}{3}(q^c q_c). \tag{C4}$$

Appendix D: Gell-Mann–Okubo relations for charmed baryons

Below, we derive the expressions for the mass dependence of each state within a multiplet up to first order in the flavor symmetry violating parameter δm_ℓ. In Eq. (7) we have matrix elements of tensor operators between tensor states

$$\langle B_R | H | B_R \rangle, \tag{D1}$$

where the baryons B and the Hamiltonian H are in the irreducible representations R and T_H, respectively. Of interest are $R = \mathbf{6}, \mathbf{3}, \overline{\mathbf{3}}$ and $T_H = \mathbf{1}, \mathbf{8}$. All the indices of the representations must be contracted, i.e., in combination they form the trivial representation. Thus, the number of terms each matrix element can depend on is equal to the number of times the singlet representation appears in the decomposition of the direct product $\overline{\mathbf{R}} \otimes \mathbf{T_H} \otimes \mathbf{R}$ [12]. For the combinations of interest, illustrated below, there is only a single instance of $\mathbf{1}$ in the direct products.

In the following, for each representation we first consider $\overline{\mathbf{R}} \otimes \mathbf{R}$ and then the direct product with T_H.

_____

[12] This is a generalization of the Wigner-Eckart theorem.

- **Sextet**: corresponding to the singly charmed baryons with $J = \frac{1}{2}^{\pm}$ or $J = \frac{3}{2}^{\pm}$. We have

$$\overline{\mathbf{R}} \otimes \mathbf{R} = \mathbf{6} \otimes \overline{\mathbf{6}} = \mathbf{1} \oplus \mathbf{8} \oplus \mathbf{27} \tag{D2}$$

The $\mathbf{6}$ representation is constructed from components of the fundamental representation, $S^{ab} = (q^a q^b + q^b q^a)$, where $q^a = (u, d, s)$. Taking the example of the $J = \frac{1}{2}^+$ sextet, we can assign the singly charmed baryons to the elements of S^{ab}:

$$\begin{aligned}
S^{11} &= 2uu \sim 2\Sigma_c^{++}, & S^{22} &= 2dd \sim 2\Sigma_c^0, \\
S^{12} &= S^{21} = (ud + du) \sim \sqrt{2}\Sigma_c^+, & S^{23} &= S^{32} = (ds + sd) \sim \sqrt{2}\Xi_c^{\prime 0}, \\
S^{13} &= S^{31} = (us + su) \sim \sqrt{2}\Xi_c^{\prime +}, & S^{33} &= 2ss \sim 2\Omega_c^0.
\end{aligned} \tag{D3}$$

The tensor product of S^{ab} with its conjugate representation, S_{cd} can be decomposed in terms of a singlet (S), octet (O_b^a) and 27-plet (T_{ab}^{cd}).

$$\mathbf{6} \otimes \overline{\mathbf{6}}: \quad S_{ab}S^{cd} = \frac{5}{72}\left\{\delta_a^c \delta_b^d + \delta_a^d \delta_b^c\right\} S + \frac{1}{6}\left\{\delta_a^c O_b^d + \delta_a^d O_b^c + \delta_b^c O_a^d + \delta_b^d O_a^c\right\} + T_{ab}^{cd}, \tag{D4}$$

with

$$\begin{aligned}
S &= S_{ef}S^{fe} \\
O_a^b &= S_{ae}S^{eb} - \frac{1}{3}\delta_a^b(S_{ef}S^{fe}) \\
T_{ab}^{cd} &= S_{ab}S^{cd} - \frac{1}{6}\left\{\delta_a^c(S_{be}S^{ed}) + \delta_a^d(S_{be}S^{ec}) + \delta_b^c(S_{ae}S^{ed}) + \delta_b^d(S_{ae}S^{ec})\right\} + \frac{1}{24}\left\{\delta_a^c \delta_b^d + \delta_a^d \delta_b^c\right\} S,
\end{aligned} \tag{D5}$$

where the summation over repeated indices is understood.

We can now identify the singlet representation that appears in the product $\overline{\mathbf{6}} \otimes \mathbf{T_H} \otimes \mathbf{6}$ and the expressions for the matrix elements. For $\mathbf{T_H} = \mathbf{1}$ we simply obtain the singlet term appearing in Eq. (D4). Thus, the lowest order term in the expansion in δm_ℓ (cf. Eq. (7)) is given by

$$\overline{m}\langle B_{\overline{\mathbf{6}}}|H_0|B_{\mathbf{6}}\rangle = M_0^{\mathbf{6}}\left[|\Sigma_c^{++}|^2 + |\Sigma_c^+|^2 + |\Sigma_c^0|^2 + |\Xi_c^{\prime +}|^2 + |\Xi_c^{\prime 0}|^2 + |\Omega_c^0|^2\right]. \tag{D6}$$

The coefficient $M_0^{\mathbf{6}}$ is the mass of the sextet in the flavor symmetric limit.

For the next order term, $H_8 \propto T_8 \propto O_3^3$, where T_8 is the second diagonal SU(3) generator and O is the octet representation ($\mathbf{T_H} = \mathbf{8} = \overline{\mathbf{8}}$). In the direct product $\overline{\mathbf{6}} \otimes \mathbf{8} \otimes \mathbf{6} = \mathbf{8} \otimes (\mathbf{1} \oplus \mathbf{8} \oplus \mathbf{27})$ the singlet appears in the $\mathbf{8} \otimes \mathbf{8}$ term. More explicitly, one contracts O_3^3 from the Hamiltonian with the $O_3^3 = S_{3c}S^{c3} - \frac{1}{3}S_{cd}S^{dc}$ part of the tensor product of the baryon representations in Eq. (D4):

$$\delta m_\ell \langle B_{\overline{\mathbf{6}}}|H_8|B_{\mathbf{6}}\rangle = \delta m_\ell \frac{A_1}{2}\left[-\frac{4}{3}\left(|\Sigma_c^{++}|^2 + |\Sigma_c^+|^2 + |\Sigma_c^0|^2\right) + \frac{2}{3}\left(|\Xi_c^{\prime +}|^2 + |\Xi_c^{\prime 0}|^2\right) + \frac{8}{3}|\Omega_c^0|^2\right]. \tag{D7}$$

Note that all particles in the sextet have the same coefficient, A_1, for this $O(\delta m_\ell)$ term modulo factors that are proportional to the light hypercharge. Isolating the mass terms for each particle up to first order in the Taylor expansion and taking the isospin limit (i.e. dropping the superscripts for the electric charges), we arrive at

$$\begin{aligned}
M_{\Sigma_c} &= M_0^{\mathbf{6}} - \frac{2}{3}A_1 \delta m_\ell + O(\delta m_\ell^2), \\
M_{\Xi_c} &= M_0^{\mathbf{6}} + \frac{1}{3}A_1 \delta m_\ell + O(\delta m_\ell^2), \\
M_{\Omega_c} &= M_0^{\mathbf{6}} + \frac{4}{3}A_1 \delta m_\ell + O(\delta m_\ell^2).
\end{aligned} \tag{D8}$$

The same expressions, but with different coefficients in each case, can be used for the other sextets.

- **Triplet**: corresponding to the doubly charmed baryons with $J = \frac{1}{2}^{\pm}$ or $J = \frac{3}{2}^{\pm}$. We proceed in an analogous way to the above starting with $\overline{\mathbf{R}} \otimes \mathbf{R} = \mathbf{3} \otimes \overline{\mathbf{3}} = \mathbf{8} \oplus \mathbf{1}$. The assignment of the components of the fundamental ($\mathbf{3}$) representation to the corresponding doubly charmed baryons is straightforward. For the example of $J = \frac{1}{2}^+$,

$$q^1 = u \sim \Xi_{cc}^{++}, \quad q^2 = d \sim \Xi_{cc}^+, \quad q^3 = s \sim \Omega_{cc}^+. \tag{D9}$$

The tensor product of q^a with the conjugate representation q_b takes the form

$$\mathbf{3} \otimes \overline{\mathbf{3}}: \quad q^a q_b = \tfrac{1}{3} \delta_b^a S + O_b^a. \tag{D10}$$

For the lowest order matrix element, corresponding to $\mathbf{T_H = 1}$, we find

$$\overline{m} \langle B_{\overline{\mathbf{3}}} | H_0 | B_{\mathbf{3}} \rangle = M_0^{\mathbf{3}} \left[|\Xi_{cc}^{++}|^2 + |\Xi_{cc}^{+}|^2 + |\Omega_{cc}^{+}|^2 \right], \tag{D11}$$

corresponding to the singlet appearing in Eq. (D10), while at the next order with $\mathbf{T_H = 8}$

$$\delta m_\ell \langle B_{\overline{\mathbf{3}}} | H_8 | B_{\mathbf{3}} \rangle = \delta m_\ell B_1 \left[-\tfrac{1}{3} (|\Xi_{cc}^{++}|^2 + |\Xi_{cc}^{+}|^2) + \tfrac{2}{3} |\Omega_{cc}^{+}|^2 \right], \tag{D12}$$

arising from contracting O_3^3 from the Hamiltonian with $O_3^3 = q^3 q_3 - \tfrac{1}{3} q^c q_c$ from Eq. (D10).

Considering the individual states we arrive at the following Gell-Mann–Okubo relations for the doubly charmed baryons,

$$\begin{aligned}
M_{\Xi_{cc}} &= M_0^{\mathbf{3}} - \tfrac{1}{3} B_1 \delta m_\ell + \mathrm{O}(\delta m_\ell^2), \\
M_{\Omega_{cc}} &= M_0^{\mathbf{3}} + \tfrac{2}{3} B_1 \delta m_\ell + \mathrm{O}(\delta m_\ell^2).
\end{aligned} \tag{D13}$$

As before, the same expressions apply to the other triplets but with different coefficients.

- **Anti-triplet**: corresponding to the singly charmed baryons with $J = \tfrac{1}{2}^{\pm}$. Here $\overline{\mathbf{R}} \otimes \mathbf{R}$ is the same as for the triplet. We construct the $\overline{\mathbf{3}}$ representation from the $\mathbf{3}$, $q_c = \epsilon_{cab} q^a q^b$, leading to the components,

$$q_1 = (ds - sd) \sim \Xi_c^0, \quad q_2 = (us - su) \sim \Xi_c^+, \quad q_3 = (ud - du) \sim \Lambda_c^+, \tag{D14}$$

in terms of the corresponding singly charmed baryons. Using this and the tensor product, $q^a q_b$, given in Eqs. (D10) we can derive the expressions, as above, for the Taylor expansion

$$\begin{aligned}
M_{\Lambda_c} &= M_0^{\overline{\mathbf{3}}} - \tfrac{2}{3} C_1 \delta m_\ell + \mathrm{O}(\delta m_\ell^2), \\
M_{\Xi_c} &= M_0^{\overline{\mathbf{3}}} + \tfrac{1}{3} C_1 \delta m_\ell + \mathrm{O}(\delta m_\ell^2).
\end{aligned} \tag{D15}$$

Appendix E: Fitting and extrapolation details

The fitting ranges chosen to extract the charmed baryon masses and the charmonium, D and D_s spectra are given in Tables XI and XII, respectively. Also included are the fits employed in the extrapolation to $\delta m_\ell^{\text{phys}}$ that are used to compute the physical point result, see Eqs. (17) and (18). Similarly, for the baryon mass differences in Table XIII. In Table XIV, we provide the coefficients extracted from linear and quadratic fits using the GMO formulae (Eqs. (10) to (16)) and their less constrained counter-parts (denoted LC1 and LC2) for the multiplets appearing in Fig. 14.

Particle	P	Operator	First eigenvalue		Second eigenvalue	
			Fit-range	Extrapolation	Fit-range	Extrapolation
Σ_c	$+$		$[10-24]_{N_f=3}$, $[10-18]_{M_\pi=255\,\text{MeV}}$			
Ξ_c'	$+$	SU(4)	$[10-24]$	GMO2, LC1,LC2	$[9-13]$	GMO1,GMO2
Ω_c	$+$					
Λ_c	$+$	SU(4)	$[11-22]$	GMO1, GMO2	$[7-13]$	GMO1, GMO2
Ξ_c	$+$					
Ξ_{cc}	$+$	SU(4)	$[11-24]$	GMO2, LC1,LC2	$[10-20]$	GMO1, GMO2
Ω_{cc}	$+$					
Σ_c	$+$					
Ξ_c'	$+$	HQET	$[10-19]$	GMO1, GMO2	$[9-16]$	GMO1, GMO2
Ω_c	$+$					
Λ_c	$+$	HQET	$[11-22]$	GMO1, GMO2	$[7-13]$	GMO1, GMO2
Ξ_c	$+$					
Ξ_{cc}	$+$	HQET	$[11-25]$	GMO2, LC1, LC2	$[10-20]$	GMO1, GMO2
Ω_{cc}	$+$					
Σ_c^*	$+$					
Ξ_c^*	$+$	HQET	$[10-20]$	GMO1, GMO2	$[9-13]$	GMO1, GMO2
Ω_c^*	$+$					
Ξ_{cc}^*	$+$	HQET	$[10-25]$	GMO1, GMO2	$[10-20]$	GMO1, GMO2
Ω_{cc}^*	$+$					
Σ_c	$-$					
Ξ_c'	$-$	SU(4)	$[10-15]$	GMO1, GMO2		
Ω_c	$-$					
Ξ_{cc}	$-$	SU(4)			$[8-13]$	GMO1, GMO2
Ω_{cc}	$-$					
Λ_c	$-$	HQET	$[11-15]$	LC1, LC2		
Ξ_c	$-$					
Ξ_{cc}	$-$	HQET	$[10-16]$	GMO2,LC1, LC2		
Ω_{cc}	$-$					
Σ_c^*	$-$					
Ξ_c^*	$-$	HQET	$[10-16]$	GMO1, GMO2		
Ω_c^*	$-$					
Ξ_{cc}^*	$-$	HQET	$[9-15]$	LC1, LC2	$[7-13]$	LC1, LC2
Ω_{cc}^*	$-$					

TABLE XI. Fitting ranges used to extract the charmed baryon masses and the fit functions employed for computing the final results at the physical point (see Section VI C) for the $32^3 \times 64$ ensembles. Note that for the negative parity states we only give details for the operators for which reliable signals could be obtained.

Particle	J^{PC}	First eigenvalue Fit-range	First eigenvalue Extrapolation	Second eigenvalue Fit-range	Second eigenvalue Extrapolation
η_c	0^{-+}	15-23	FS1, FS2	10-17	FS1, FS2
J/ψ	1^{--}	15-23	FS1, FS2	10-17	FS1, FS2
χ_{c0}	0^{++}	15-27	FS1, FS2		
χ_{c1}	1^{++}	15-27	FS1, FS2		
h_c	1^{+-}	13-27	FS1, FS2		
D D_s	0^-	15-26	GMO2, LC1, LC2		
D^* (D_s^*)	1^-	15-26	GMO1, GMO2		
$\bar{c}l$ $\bar{c}s\,(D_{s0}^*)$	0^+	10-15	NC1, NC2 NC1, NC2		
$(\bar{c}\gamma_i\gamma_5 l),(\bar{c}\epsilon_{ijk}\gamma_j\gamma_k l)$ $(\bar{c}\gamma_i\gamma_5 s),(\bar{c}\epsilon_{ijk}\gamma_j\gamma_k s)$	1^+	10-14	NC1, NC2 NC1, NC2	10-14	NC1, NC2 NC1, NC2

TABLE XII. As in Table XI for the lower lying meson channels. The extrapolations FS1 and FS2 refer to flavour singlet fits which include a constant term and a constant plus a quadratic (δm_ℓ^2) term, respectively. Similarly, NC1 and NC2 denote a linear fit to a single channel and a linear plus quadratic fit, respectively. The GMO and LC fits are defined in the Section VI B.

Difference	Operator	Extrapolation
Spin splittings		
$\Sigma_c^* - \Sigma_c, \Xi_c^* - \Xi_c, \Omega_c^* - \Omega_c$	HQET	GMO1, GMO2
$\Xi_{cc}^* - \Xi_{cc}, \Omega_{cc}^* - \Omega_{cc}$	HQET	GMO2, LC1, LC2
Structure splittings		
$\Sigma_c - \Lambda_c, \Xi_c' - \Xi_c$	SU(4)	GMO1, GMO2
$\Sigma_c - \Lambda_c, \Xi_c' - \Xi_c$	HQET	GMO1, GMO2
Flavour splittings $s \to u/d$		
$\Xi_c' - \Sigma_c, \Omega_c - \Xi_c', \Omega_c - \Sigma_c$	SU(4)	GMO1, GMO2
$\Xi_c' - \Sigma_c, \Omega_c - \Xi_c', \Omega_c - \Sigma_c$	HQET	GMO1, GMO2
$\Xi_c - \Lambda_c$	SU(4)	LC1, LC2
$\Xi_c - \Lambda_c$	HQET	LC1, LC2
$\Omega_{cc} - \Xi_{cc}$	SU(4)	LC1, LC2
$\Omega_{cc} - \Xi_{cc}$	HQET	LC1, LC2
$\Xi_c^* - \Sigma_c^*, \Omega_c^* - \Xi_c^*, \Omega_c^* - \Sigma_c^*$	HQET	GMO1, GMO2
Flavour splittings $c \to u/d$ and $c \to s$		
$\Omega_{cc} - \Omega_c, \Xi_{cc} - \Xi_c', \Xi_{cc} - \Sigma_c, \Omega_{cc} - \Xi_c'$	SU(4)	GMO1, GMO2
$\Omega_{cc} - \Omega_c, \Xi_{cc} - \Xi_c', \Xi_{cc} - \Sigma_c, \Omega_{cc} - \Xi_c'$	HQET	GMO1, GMO2
$\Omega_{cc}^* - \Omega_c^*, \Xi_{cc}^* - \Xi_c^*, \Xi_{cc}^* - \Sigma_c^*, \Omega_{cc}^* - \Xi_c^*$	HQET	GMO1, GMO2

TABLE XIII. The fit functions used for the extrapolation of the positive parity ground state differences to δm_l^{phys}. The splittings listed together were fitted simultaneously. Note that for $\Xi_c - \Lambda_c$ and $\Omega_{cc} - \Xi_{cc}$, there are no corresponding GMO expressions, since these are splittings between multiplets containing two states.

Sextet SU(4) $J = \frac{1}{2}^+$, $(\Sigma_c, \Xi'_c, \Omega_c)$

LC1			LC2			GMO2	
$M^{\mathbf{6}}_{0(LC1)}$	2.5530(59)		$M^{\mathbf{6}}_{0(LC2)}$	2.5502(66)		$M^{\mathbf{6}}_{0(GMO2)}$	2.5509(57)
$A_{1(LC1)}$	−0.1428(153)		$A_{1(LC2)}$	−0.0921(601)		$A_{1(GMO2)}$	0.3006(282)
$A'_{1(LC1)}$	0.0232(127)		$A'_{1(LC2)}$	0.0720(497)		$A_{2(GMO2)}$	−0.0688(344)
$A''_{1(LC1)}$	0.1740(115)		$A''_{1(LC2)}$	0.2155(422)		$A_{3(GMO2)}$	−0.0382(181)
			$A_{2(LC2)}$	−0.0744(941)		$A_{4(GMO2)}$	−0.0372(273)
			$A_{3(LC2)}$	−0.0715(723)			
			$A_{4(LC2)}$	−0.0592(576)			

Sextet SU(4) $J^P = \frac{1}{2}^-$, $(\Sigma_c, \Xi'_c, \Omega_c)$

GMO1			GMO2	
$M^{\mathbf{6}}_{0(GMO1)}$	2.8650(160)		$M^{\mathbf{6}}_{0(GMO2)}$	2.9080(239)
$A_{1(GMO1)}$	0.3383(300)		$A_{1(GMO2)}$	0.0312(1065)
			$A_{2(GMO2)}$	−0.4212(1391)
			$A_{3(GMO2)}$	−0.0875(734)
			$A_{4(GMO2)}$	0.2048(1019)

Triplet HQET $J^P = \frac{1}{2}^+$, (Ξ_{cc}, Ω_{cc})

LC1			LC2			GMO2	
$M^{\mathbf{3}}_{0(LC1)}$	3.6585(44)		$M^{\mathbf{3}}_{0(LC2)}$	3.6596(48)		$M^{\mathbf{3}}_{0(GMO2)}$	3.6559(40)
$B_{1(LC1)}$	0.0723(89)		$B_{1(LC2)}$	0.0557(305)		$B_{1(GMO2)}$	−0.0471(46)
$B''_{1(LC1)}$	−0.0729(99)		$B''_{1(LC2)}$	−0.0955(369)		$B_{2(GMO2)}$	−0.0271(164)
			$B_{2(LC2)}$	0.0242(420)		$B_{3(GMO2)}$	−0.0330(199)
			$B_{3(LC2)}$	0.0349(551)			

Triplet HQET $J^P = \frac{1}{2}^-$, (Ξ_{cc}, Ω_{cc})

LC1			LC2			GMO2	
$M^{\mathbf{3}}_{0(LC1)}$	4.0143(191)		$M^{\mathbf{3}}_{0(LC2)}$	4.0281(216)		$M^{\mathbf{3}}_{0(GMO2)}$	4.0158(172)
$B_{1(LC1)}$	0.0559(392)		$B_{1(LC2)}$	−0.0817(1274)		$B_{1(GMO2)}$	−0.0152(227)
$B''_{1(LC1)}$	−0.1580(445)		$B''_{1(LC2)}$	−0.1611(1568)		$B_{2(GMO2)}$	0.0435(759)
			$B_{2(LC2)}$	0.1897(1730)		$B_{3(GMO2)}$	−0.2641(908)
			$B_{3(LC2)}$	−0.0605(2348)			

Antitriplet SU(4) $J^P = \frac{1}{2}^+$, (Λ_c, Ξ_c)

GMO1			GMO2	
$M^{\overline{\mathbf{3}}}_{0(GMO1)}$	2.4274(40)		$M^{\overline{\mathbf{3}}}_{0(GMO2)}$	2.4337(56)
$C_{1(GMO1)}$	0.0756(25)		$C_{1(GMO2)}$	0.0817(90)
			$C_{2(GMO2)}$	−0.0099(537)
			$C_{3(GMO2)}$	−0.0429(205)

Antitriplet HQET $J^P = \frac{1}{2}^-$, (Λ_c, Ξ_c)

LC1			LC2	
$M^{\overline{\mathbf{3}}}_{0(LC1)}$	2.7825(332)		$M^{\overline{\mathbf{3}}}_{0(LC2)}$	2.8002(356)
$C_{1(LC1)}$	−0.3500(936)		$C_{1(LC2)}$	−0.9128(3261)
$C'_{1(LC1)}$	−0.0276(783)		$C'_{1(LC2)}$	−0.3978(2514)
			$C_{2(LC2)}$	1.0029(5636)
			$C_{3(LC2)}$	0.5979(3759)

TABLE XIV. The coefficients determined from linear and quadratic GMO and LC fits (see Section VI B) to the ground state positive and negative parity multiplets displayed in Fig. 14.

[1] N. Isgur and M. B. Wise, Phys. Lett. **B232**, 113 (1989).
[2] E. Eichten and B. R. Hill, Phys. Lett. **B234**, 511 (1990).
[3] W. Caswell and G. Lepage, Phys. Lett. **B167**, 437 (1986).
[4] G. T. Bodwin, E. Braaten, and G. P. Lepage, Phys. Rev. **D51**, 1125 (1995), arXiv:hep-ph/9407339 [hep-ph].
[5] A. Pineda and J. Soto, Nucl. Phys. Proc. Suppl. **64**, 428 (1998), arXiv:hep-ph/9707481 [hep-ph].
[6] N. Brambilla, A. Pineda, J. Soto, and A. Vairo, Nucl. Phys. **B566**, 275 (2000), arXiv:hep-ph/9907240 [hep-ph].
[7] K. Olive *et al.* (Particle Data Group), Chin. Phys. **C38**, 090001 (2014).
[8] E. Cazzoli *et al.*, Phys. Rev. Lett. **34**, 1125 (1975).
[9] B. Knapp *et al.*, Phys. Rev. Lett. **37**, 882 (1976).
[10] M. Basile *et al.*, Lett. Nuovo Cim. **31**, 97 (1981).
[11] M. Mattson *et al.* (SELEX), Phys. Rev. Lett. **89**, 112001 (2002).
[12] A. Ocherashvili *et al.* (SELEX), Phys. Lett. **B628**, 18 (2005), arXiv:hep-ex/0406033 [hep-ex].
[13] J. Russ (SELEX)(2002), arXiv:hep-ex/0209075 [hep-ex].
[14] L. Copley, N. Isgur, and G. Karl, Phys. Rev. **D20**, 768 (1979).
[15] S. Capstick and N. Isgur, Phys. Rev. **D34**, 2809 (1986).
[16] R. Roncaglia, D. Lichtenberg, and E. Predazzi, Phys. Rev. **D52**, 1722 (1995).
[17] B. Silvestre-Brac, Few Body Syst. **20**, 1 (1996).
[18] D. Ebert, R. Faustov, V. Galkin, and A. Martynenko, Phys. Rev. **D66**, 014008 (2002).
[19] D. Ebert, R. Faustov, and V. Galkin, Phys. Rev. **D72**, 034026 (2005).
[20] W. Roberts and M. Pervin, Int. J. Mod. Phys. **A23**, 2817 (2008).
[21] H. Garcilazo, J. Vijande, and A. Valcarce, J. Phys. **G34**, 961 (2007).
[22] A. Valcarce, H. Garcilazo, and J. Vijande, Eur. Phys. J. **A37**, 217 (2008).
[23] E. E. Jenkins, Phys. Lett. **B315**, 447 (1993).
[24] E. Bagan, M. Chabab, H. G. Dosch, and S. Narison, Phys. Lett. **B278**, 367 (1992).
[25] E. Bagan, M. Chabab, H. G. Dosch, and S. Narison, Phys. Lett. **B287**, 176 (1992).
[26] D.-W. Wang, M.-Q. Huang, and C.-Z. Li, Phys. Rev. **D65**, 094036 (2002).
[27] Z.-G. Wang, Eur. Phys. J. **C54**, 231 (2008).
[28] J.-R. Zhang and M.-Q. Huang, Phys. Rev. **D78**, 094007 (2008), arXiv:0810.5396 [hep-ph].
[29] J.-R. Zhang and M.-Q. Huang, Phys. Rev. **D78**, 094015 (2008), arXiv:0811.3266 [hep-ph].
[30] K. Bowler *et al.* (UKQCD), Phys. Rev. **D54**, 3619 (1996), arXiv:hep-lat/9601022 [hep-lat].
[31] J. Flynn, F. Mescia, and A. S. B. Tariq (UKQCD), JHEP **0307**, 066 (2003), arXiv:hep-lat/0307025 [hep-lat].
[32] N. Mathur, R. Lewis, and R. Woloshyn, Phys. Rev. **D66**, 014502 (2002), arXiv:hep-ph/0203253 [hep-ph].
[33] R. Lewis, N. Mathur, and R. Woloshyn, Phys. Rev. **D64**, 094509 (2001), arXiv:hep-ph/0107037 [hep-ph].
[34] T.-W. Chiu and T.-H. Hsieh, Nucl. Phys. **A755**, 471 (2005), arXiv:hep-lat/0501021 [hep-lat].
[35] H. Na and S. A. Gottlieb, PoS **LAT2007**, 124 (2007).
[36] L. Liu, H.-W. Lin, K. Orginos, and A. Walker-Loud, Phys. Rev. **D81**, 094505 (2010).
[37] R. A. Briceño, H.-W. Lin, and D. R. Bolton, Phys. Rev. **D86**, 094504 (2012), arXiv:1207.3536 [hep-lat].
[38] C. Alexandrou, J. Carbonell, D. Christaras, V. Drach, M. Gravina, and M. Papinutto (ETMC), Phys. Rev. **D86**, 114501 (2012), arXiv:1205.6856 [hep-lat].
[39] S. Basak, S. Datta, M. Padmanath, P. Majumdar, and N. Mathur (ILGTI), PoS **LATTICE2012**, 141 (2012), arXiv:1211.6277 [hep-lat].
[40] S. Dürr, G. Koutsou, and T. Lippert, Phys. Rev. **D86**, 114514 (2012), arXiv:1208.6270 [hep-lat].
[41] Y. Namekawa *et al.* (PACS-CS), Phys. Rev. **D87**, 094512 (2013), arXiv:1301.4743 [hep-lat].
[42] C. Alexandrou, V. Drach, K. Jansen, C. Kallidonis, and G. Koutsou (ETMC), Phys. Rev. **D90**, 074501 (2014), arXiv:1406.4310 [hep-lat].
[43] Z. S. Brown, W. Detmold, S. Meinel, and K. Orginos, Phys. Rev. **D90**, 094507 (2014), arXiv:1409.0497 [hep-lat].
[44] M. Padmanath, R. G. Edwards, N. Mathur, and M. Peardon (HSC)(2015), arXiv:1502.01845 [hep-lat].
[45] M. Gell-Mann, Phys. Rev. **125**, 1067 (1962).
[46] S. Okubo, Prog. Theor. Phys. **27**, 949 (1962).
[47] S. Dürr(2014), arXiv:1412.6434 [hep-lat].
[48] W. Bietenholz *et al.* (QCDSF), Phys. Lett. **B690**, 436 (2010).
[49] W. Bietenholz *et al.* (QCDSF), Phys. Rev. **D84**, 054509 (2011).
[50] M. Bruno *et al.*, JHEP **1502**, 043 (2015), arXiv:1411.3982 [hep-lat].
[51] N. Cundy *et al.*, Phys. Rev. **D79**, 094507 (2009).
[52] R. Sommer, Nucl.Phys. **B411**, 839 (1994), arXiv:hep-lat/9310022 [hep-lat].
[53] S. Borsanyi *et al.*, JHEP **1209**, 010 (2012), arXiv:1203.4469 [hep-lat].
[54] M. Lüscher, JHEP **1008**, 071 (2010), arXiv:1006.4518 [hep-lat].
[55] R. Horsley, J. Najjar, Y. Nakamura, H. Perlt, D. Pleiter, P. E. L. Rakow, G. Schierholz, A. Schiller, H. Stüben, and J. M. Zanotti (QCDSF), PoS **LATTICE2013**, 249 (2013), arXiv:1311.5010 [hep-lat].
[56] G. S. Bali and P. Boyle, Phys. Rev. **D59**, 114504 (1999), arXiv:hep-lat/9809180 [hep-lat].
[57] M. A. Nowak, M. Rho, and I. Zahed, Phys. Rev. **D48**, 4370 (1993), arXiv:hep-ph/9209272 [hep-ph].
[58] W. A. Bardeen and C. T. Hill, Phys. Rev. **D49**, 409 (1994), arXiv:hep-ph/9304265 [hep-ph].
[59] D. Ebert, T. Feldmann, R. Friedrich, and H. Reinhardt, Nucl. Phys. **B434**, 619 (1995), arXiv:hep-ph/9406220 [hep-ph].

[60] D. Mohler, S. Prelovsek, and R. Woloshyn, Phys. Rev. **D87**, 034501 (2013), arXiv:1208.4059 [hep-lat]

[61] C. Lang, L. Leskovec, D. Mohler, S. Prelovsek, and R. Woloshyn, Phys. Rev. **D90**, 034510 (2014), arXiv:1403.8103 [hep-lat]

[62] V. Crede and W. Roberts, Rept. Prog. Phys. **76**, 076301 (2013), arXiv:1302.7299 [nucl-ex]

[63] N. Brambilla, A. Vairo, and T. Rosch, Phys. Rev. **D72**, 034021 (2005), arXiv:hep-ph/0506065 [hep-ph]

[64] C. Michael, Nucl. Phys. **B259**, 58 (1985)

[65] M. Lüscher and U. Wolff, Nucl. Phys. **B339**, 222 (1990)

[66] B. Blossier, M. Della Morte, G. von Hippel, T. Mendes, and R. Sommer, JHEP **0904**, 094 (2009), arXiv:0902.1265 [hep-lat]

[67] S. Güsken, U. Löw, K. Mütter, R. Sommer, A. Patel, and K. Schilling, Phys. Lett. **B227**, 266 (1989)

[68] S. Güsken, Nucl. Phys. Proc. Suppl. **17**, 361 (1990)

[69] M. Falcioni, M. Paciello, G. Parisi, and B. Taglienti, Nucl. Phys. **B251**, 624 (1985)

[70] M. Albanese *et al.* (APE), Phys. Lett. **B192**, 163 (1987)

[71] U. Wolff (ALPHA), Comput. Phys. Commun. **156**, 143 (2004), arXiv:hep-lat/0306017 [hep-lat]

[72] S. Schäfer, R. Sommer, and F. Virotta (ALPHA), Nucl. Phys. **B845**, 93 (2011), arXiv:1009.5228 [hep-lat]

[73] A. X. El-Khadra, A. S. Kronfeld, and P. B. Mackenzie, Phys. Rev. **D55**, 3933 (1997), arXiv:hep-lat/9604004 [hep-lat]

[74] S. Aoki, Y. Kuramashi, and S.-i. Tominaga, Prog. Theor. Phys. **109**, 383 (2003), arXiv:hep-lat/0107009 [hep-lat]

[75] N. H. Christ, M. Li, and H.-W. Lin, Phys. Rev. **D76**, 074505 (2007), arXiv:hep-lat/0608006 [hep-lat]

[76] R. Frezzotti, P. A. Grassi, S. Sint, and P. Weisz (ALPHA), JHEP **0108**, 058 (2001), arXiv:hep-lat/0101001 [hep-lat]

[77] L. Liu, G. Moir, M. Peardon, S. M. Ryan, C. E. Thomas, P. Vilaseca, J. J. Dudek, R. G. Edwards, B. Joo, and D. G. Richards (HSC), JHEP **1207**, 126 (2012), arXiv:1204.5425 [hep-ph]

[78] H. Neuberger, Phys. Lett. **B417**, 141 (1998), arXiv:hep-lat/9707022 [hep-lat]

[79] C. Bernard, T. Burch, T. A. DeGrand, S. Datta, C. DeTar, S. Gottlieb, U. M. Heller, K. Orginos, R. Sugar, and D. Toussaint, Phys. Rev. **D64**, 054506 (2001), arXiv:hep-lat/0104002 [hep-lat]

[80] A. Bazavov *et al.* (MILC), Phys. Rev. **D82**, 074501 (2010), arXiv:1004.0342 [hep-lat]

[81] W. Bietenholz, M. Göckeler, R. Horsley, Y. Nakamura, D. Pleiter, P. E. L. Rakow, G. Schierholz, and J. M. Zanotti, Phys. Lett. **B687**, 410 (2010), arXiv:1002.1696 [hep-lat]

[82] S. Aoki *et al.* (PACS-CS), Phys. Rev. **D81**, 074503 (2010), arXiv:0911.2561 [hep-lat]

[83] Y. Aoki *et al.* (RBC, UKQCD), Phys. Rev. **D83**, 074508 (2011), arXiv:1011.0892 [hep-lat]

[84] S. Borsanyi *et al.*(2014), arXiv:1406.4088 [hep-lat]

[85] W. Söldner (RQCD)(2015), arXiv:1502.05481 [hep-lat]

[86] R. G. Edwards and B. Joò (SciDAC , LHPC , UKQCD), Nucl. Phys. Proc. Suppl. **140**, 832 (2005)